General comment on paper ACPD-2015-215

Interactions among drainage flows, gravity waves and turbulence: a BLLAST case study, by C. Román-Cascón et al.

Dear Editor,

On behalf of the coauthors of the manuscript ACPD-2015-215 and after the discussion stage of ACPD, I would like to submit a new version of this paper.

We have taken into consideration all the comments and recommendations from three anonymous reviewers and we have changed the manuscript accordingly. These comments and their responses are attached to this letter. Besides, a marked-up manuscript version showing the changes made (using latexdiff) is also attached to this letter.

Please, note also that in some occasions we cite in the manuscript these published comments in ACPD, in order to link the text of the manuscript with the debate followed during the discussion stage, since some questions are still “open questions” and they should not be included in the main text.

Following recommendations from reviewer #2, we changed the size of axes and legends in all the figures. For this reason, the changes have been applied to the original manuscript (in latex) submitted on 20 March 2015, and not directly to the typeset latex file that corresponds to the published discussion paper (which is very similar to the other). We were not able to edit the published figures but the original ones.

Although it was not a query from the reviewers, the English in the whole text has been completely revised and some expressions have changed a little bit. However, in no case these changes imply an alteration of the scientific content.

Once again, we would like to thank the three anonymous reviewers of the manuscript for their helpful comments, which undoubtedly have improved the quality of the manuscript.

We are looking forward from hearing a positive feedback from you.

Yours sincerely,

Carlos Román-Cascón

AUTHORS RESPONSE TO: *Interactive comment on "Interactions among drainage flows, gravity waves and turbulence: a BLLAST case study" by C. Román-Cascón et al.*

Anonymous Referee #1

* Answers are in blue and reviewer comments are in black. Please, note that figures in this document are indicated with * symbol, while figures of the manuscript are linked without this symbol.

This paper describes a case study from the BLLAST field campaign which focussed on formation of stable boundary layers around the evening transition in complex terrain. The case study is an interesting one where after a brief period of calm, a shallow drainage flow forms downslope, eventually overwhelmed by a larger scale nocturnal katabatic flow from the mountains to the south (which is investigated with help of a numerical model). Propagating gravity waves are detected in pressure signals at the surface during both the main phases of the flow, and in turn characterised, and impacts on surface turbulence and fluxes due to these waves and the drainage flow are examined. Multi-Resolution Flux Decomposition (MRFD) is used to elucidate effects across scales, and comparisons made for a range of heights spanning the depth of the shallow drainage flow, and for three different sites. MRFD illustrates nicely the separation of scales and, for instance, direct (wave-induced convergence/divergence) and indirect (modulation of winds and hence turbulence and fluxes as a result of convergence/divergence) influences of gravity waves. These aptly demonstrate local variability, and at times how difficult it is to explain conclusively, and the difficulty in defining averaging intervals for turbulent flux calculations. While I felt explanations in places could be a little better thought through and lucid, and perhaps more attempt made to at least tentatively explain rather than simply describe, I'm happy to recommend publication subject to carrying out minor revisions in response to the list below, expanding their analysis if the answer to a given point exposes any oversight by the authors or potential benefit of deeper examination.

The authors would like to thank Reviewer #1 for his/her helpful comments and suggestions. We are sure that they are going to improve the quality of the manuscript.

As a result of the queries from the three reviewers, the authors include a deeper explanation of some of the processes commented through the paper in the new version of the manuscript.

12824. 22. "allusive" should be "elusive".

It has been changed in the text.

12826. 6. "on the study" should be "out the study".

It has been changed in the text.

12830. 25. What instrument is shown in Figure 3?

This is also a query of Reviewer #2. These profiles were plotted from sonic measurements obtained at the divergence site tower (below 8 m) and from the 60 m tower. This information has been included in the caption.

12830. 27. It looks like there is a shallow (1m) drainage current occurring at the wheat site.

Yes, it is, but after discussion among co-authors and people on charge of the instrumentation of this tower, we concluded that the lower measurements of the edge site towers have been subject to SE flow blocking/distortion by the mast and other equipment mounted on the mast, especially during the dominant low-wind conditions. Therefore, we propose to eliminate 0.5 and 1 m levels from the figure of the grass-site tower (Figure 4a) and 1 and 1.5 m levels from the figure of the wheat-site tower (Figure 4b).

Figures 2 and (especially) 4 - it would be better if a given colour corresponded to approximately the same height in each figure panel.

We do agree. We have changed the colours in the new version of the manuscript, according to the suggestion.

Figure 8(d) - how was this BV frequency calculated? It looks rather noisy. Were adjacent pairs of heights used? If so did the authors try any methods which take into account a deeper range of heights at each level (which would, looking at Figure 8(c), presumably lead to a smoother profile of BVF)?

Yes, we calculated N_{BV} using adjacent temperature measurements. Reviewer #2 asked the same.

N_{BV} has been calculated from temperature measurements (potential temperature) at different heights. In fact, the temperature profile showed in Figure 8c is not as smooth as it seems, since it includes narrow unstable layers (and therefore some narrow layers have $N^2_{BV} < 0$ s^{-2}). Temperature above 60 m is obtained from measurements of tethered balloon descent, which was averaged **every 5 data** in the first version of the manuscript. This is the reason of the noisy behaviour of N_{BV} profile.

To solve this, a new figure has been prepared (Figure 1*, new Figure 8d), where measurements from tethered balloon are averaged **over 20 m layers** instead of over 5 data points. In this case, N_{BV} profile is smoothed, although it still has a clear layer where N^2_{BV} becomes negative, located around 200 m agl. We have changed the main text and we state that it is not so easy to determine exactly the layer where GWs are propagating, since it depends on GWs features and wind and temperature profiles. However, we also say that the propagation around the layer at 200 m agl is not going to be favoured, since the thermal profile is not stable in a shallow layer at that height.

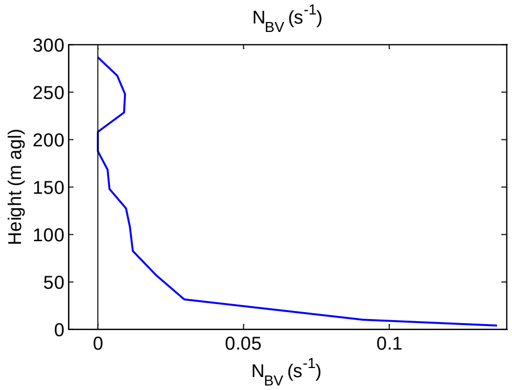

Figure 1*. Brunt-Väisälä frequency (N_{BV}) (s^{-1}) calculated every 20 meters after averaging tethered balloon data.

12833. 8. "as" should be "such as".

It has been changed in the text.

12834. 11-18. It feels as though the authors should at least make some effort to back up their assertion by helping the reader draw a visual correlation between the variables in Figures 2 and 4 and the pressure oscillations, perhaps by drawing dotted lines on the figures to indicate particular features.

The whole text has been completely revised and now we try to write more details observed in figures. It will be included with the next submission of the manuscript.

12836. 8. word missing here?

Yes. It has been changed by "...a continuous signal in the MRFD"

12389. 8. Do the authors have any explanation for the difference in wind between the grass and wheat sites during this period? Can the authors comment on the effect of the field boundary close and to the south (i.e. upwind) of the grass site? Could this play any part in the low winds experienced at the lowest detector levels during the SDF period at this site? Alternatively does the downwind wheat (and associated "flow collision") have any impact.

We do agree. The maize field located to the south (upwind) of the grass site (see Figure 2c* and 2d*) could also be influencing the low wind measured at the grass site. When the flow passes through the grass and arrives to the boundary site, turbulence is increased by collision of the flow with the boundary and then the flow is again different at the wheat, influenced by the canopy of this vegetation. This discussion is included in the new version of the manuscript.

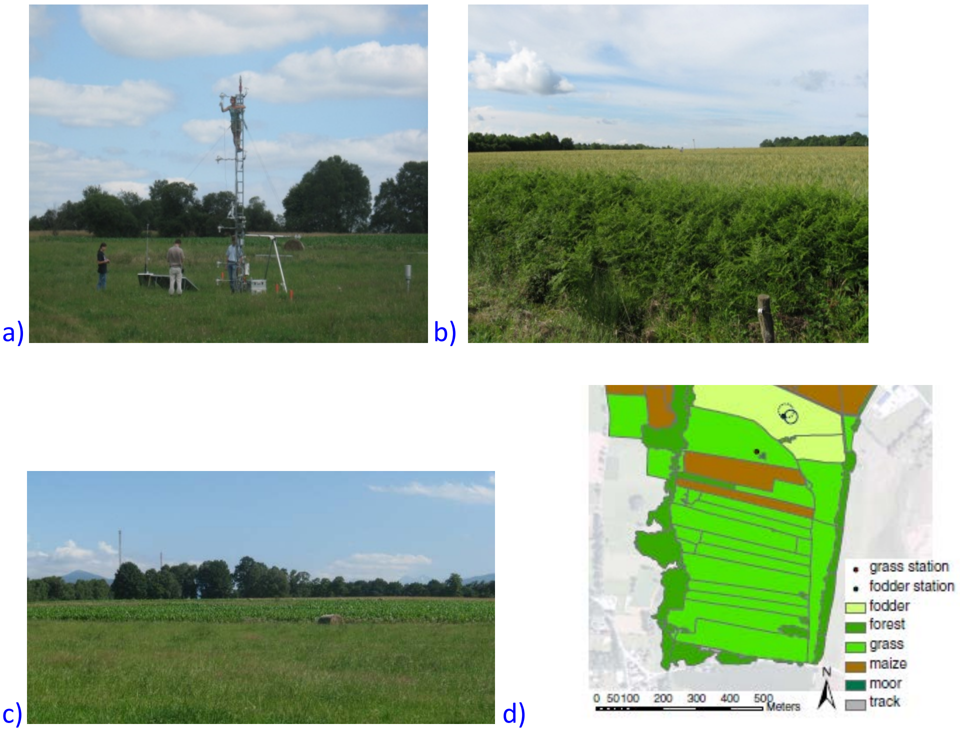

Figure 2*. a) Grass tower with line of three trees in the background (to the SE). b) Vegetation composing the boundary site (note that this kind of vegetation is harder than wheat, located in the background). c) Maize field located to the south of the grass site and line of trees at the background (SE). d) Land-use map from van de Boer et al. (2014).

REF -- Van de Boer, A., Moene, A. F., Graf, A., Schüttemeyer, D., & Simmer, C. (2014). Detection of Entrainment Influences on Surface-Layer Measurements and Extension of Monin–Obukhov Similarity Theory. Boundary-layer meteorology, 152(1), 19-44.

12839. 11. Figure number incorrect.

Yes, it was incorrect. Thank you. It has been changed to "Figure 11c".

12839. 9-20. It seems that a lot of this can be explained simply by the fact that the wind changes barely at the wheat site, but radically at the grass at the onset of the mountain-plain wind...

We do agree. This information has been added in the text.

12840. 21-24. I didn't understand this sentence, could the authors clarify?

This question was asked by reviewer #2 as well. In fact, the sentence was not correctly expressed and it has been changed following suggestions from both reviewers. We meant that the increase in turbulence caused a reduction in the temperature gradient (mixing), and therefore, the heat flux was reduced.

AUTHORS RESPONSE TO: *Interactive comment on "Interactions among drainage flows, gravity waves and turbulence: a BLLAST case study" by C. Román-Cascón et al.*

Anonymous Referee #2

* Answers are in blue and reviewer comments are in black. Please, note that figures in this document are indicated with * symbol, while figures of the manuscript are linked without this symbol.

This manuscript presents a rather nice case study from the BLLAST field campaign demonstrating the interaction between shallow drainage flows, gravity waves and turbulence in the hours around and just after sunset. Understanding, and being able to model, the complex small-scale processes which are important in stable boundaries layers over non-homogeneous terrain remains a challenging problem, and detailed observational studies such as this are an important part of talking these challenges. The MRFD technique offers an interesting way of studying the contributions to the flux from different scales in the flow. The material is certainly worthy of publication, however I do have some queries and suggestions which I hope will clarify and improve the presentation of this work.

The authors appreciate the effort done by Referee #2 reviewing this manuscript. His/her comments will improve the quality and clarity of the manuscript. In the following answers, we will try to answer to all the queries.

As a result of the queries from the three reviewers, the authors include a deeper explanation of some of the processes commented through the paper in the new version of the manuscript.

MAJOR COMMENTS

1) **p12832 and table 3.** The parameters here seem to demonstrate quite a bit of variability from one time period to the next. While this is not surprising given the complications of "real world" flows, it would be useful for the reader to 1) have a clearer idea how they were obtained and 2) give some estimate of the uncertainty in these parameters.

Sometimes we present these values with figures, which is maybe a more illustrative way than using tables (see example in Figure 1* (below) for period 20.35 to 20.55 UTC).

These figures are obtained through the calculation of phase differences between filtered surface pressure from 3 microbarometers (knowing their exact position). Thus, for different wave periods, we obtain different values and the same for different times. The range of wave periods is previously selected from regions of high energy in wavelet analysis. From this information, we plot the contours of the values and we obtain a figure like Figure 1*. In these kinds of figures, the uncertainty is determined by the range of values obtained. For example, a perfect wave (ideal) of 20-min period will have a constant value of 20-min period for the whole time period (without superimposition of other motions).

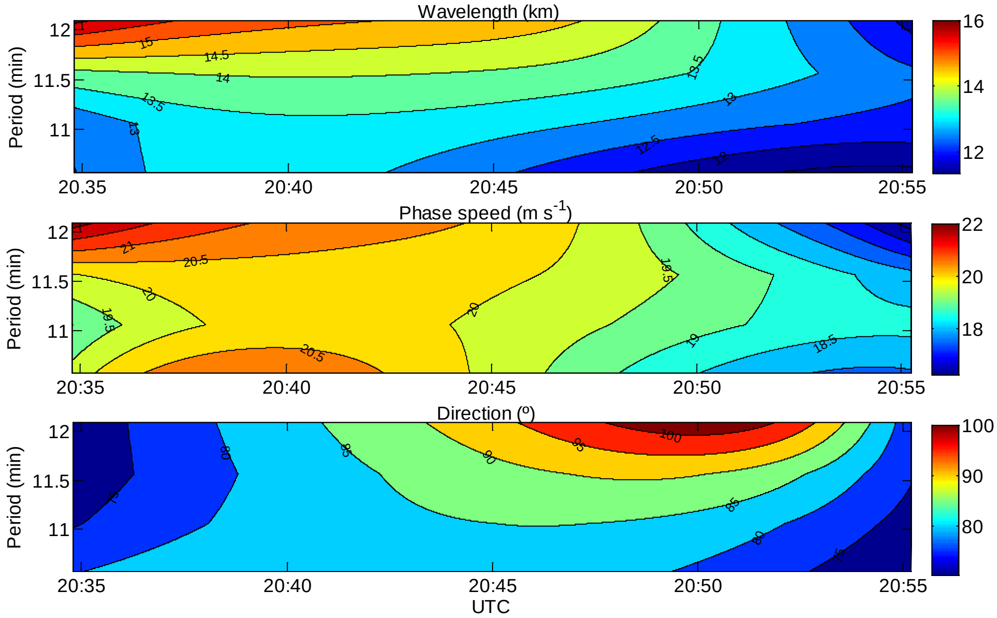

Figure 1*. Wave parameters evaluated from 20.35 UTC to 20.55 UTC and for wave periods between 10.5 and 12 minutes: a) Wavelength (km). b) Phase speed (m s^{-1}). c) Direction of propagation (º).

As stated by the reviewer, in the real world is very difficult to find near monochromatic waves, but, the shorter this range of values is, the more monochromatic a wave is.

Due to the high variability found among different periods, it is not appropriate to show a figure like Figure 1*for the whole period (approximately from 19.30 UTC to 21.30 UTC) in the manuscript, because we lose detail in the contours (large range of values for larger time periods). On the other hand, it is not the best idea to show 4 figures like Figure 1* for each period, since that would be too many figures. Thus, we concluded that the better way to show the information was in a table, where the range of values (given in "[ ]") show the variability for different times and periods. For the last two periods (20.35 to 20.55 UTC and 21.05 to 21.30 UTC), we found a relatively small range of values compared to the two first periods and to other cases previously analysed by authors. This is indicating quite clear wave parameters (short range of values). To highlight this, we gave in Table 3 (in the first manuscript) exact values for the two last periods (instead of giving a range), although it is true that there are uncertainties. We propose to include these uncertainties (range of values) for wave event 2 in a new Table 3 (see below):

	Time (UTC)	Period (min)	Wavelength (km)	Phase speed (ms^{-1})	Direction of propagation (º)
Wave event 1	1925–2000	20–25	not well defined	not well defined	not well defined
	2005–2025	22-24	[23 - 30]	[17 – 19]	[80 – 90]
Wave event 2	2035–2055	10.5-12	[12 - 15]	[18 – 20]	[75 - 95]
	2105–2130	16-21	[7 - 10]	[6 - 9]	[32 - 42]

Table 1* (new Table 3) → Gravity waves parameters evaluated from filtered surface pressure records of three microbarometers. Uncertainty is indicated inside brackets (range of values). Note how uncertainty is lower for wave event 2.

Therefore, we include now the uncertainty inside brackets in the form of range of values for all periods. In addition, a better explanation of how we calculate this is proposed to be included in the main text (at the beginning of Section 3.2.1 p12832). We also include references to Viana et al. (2009) and Terradellas et al. (2001):

"*Wave parameters have been evaluated from phase difference analysis (see Section 2.2.1), knowing the exact position of each microbarometer (Terradellas et al., 2001; Viana et al., 2009). This method is based on the differences between wave phases of the three filtered pressure records (one for each microbarometer). These differences are calculated for a determined time period and attending to different wave periods. Thus, for selected ranges of time and wave periods, we obtain specific ranges of wave parameters. The shorter this range of values is (for example for wavelength), the more monochromatic a wave is. This evaluation indicates not well defined values for the first part of Event 1 (Table 3, from 1925 to 2000 UTC). This means… (Continuation in p12832 line 5)*"

2) **p12833.** The authors seem to have a conceptual picture of the gravity wave here and how it propagates, but this is not very clearly communicated to the reader. I assume you are picturing some form of trapped gravity wave? Do the profiles of temperature and wind given in figure 8 give rise to trapped waves of the right kind of wavelength? You mention the role of shear at around 100m. Would plotting the Scorer parameter profile in figure 8 demonstrate possible wave trapping?

In the first version of the manuscript, we considered gravity waves trapped in the layer from the surface to approximately 100 m agl, where the conditions are stable without any doubt. The minimum N_{BV} found in this layer was 0.01 s^{-1}, which indicates that gravity waves of smaller frequencies can form and propagate in the layer. The maximum frequency of the analysed gravity waves is 0.0017 s^{-1} (corresponding to a period of 10 minutes). Thus, in theory, our waves can exist and propagate in the layer. Having plotted the new N_{BV} (see answer to next question), we are not really sure about the depth of the stable layer (from surface), and in the new version of the manuscript, we do not give an exact layer where GWs can be propagating (since we are not really sure).

In fact, we tried to plot the vertical wavenumber (m^2) to show possible wave trapping. However, we only have the temperature and wind profiles around 19.55 UTC (tethered balloon sounding). At this time, we were not able to obtain clear wave parameters with cross-correlation measurements. The wave parameters shows a relatively "large range" of values, indicating that the features of the waves are not very clear (see also wave parameters for wave event 1 in Table 1* (new Table 3)).

For example, if we use λ=20 km; and phase speed of 15 m s^{-1}, we obtain the vertical wavenumber (m^2) profile shown in Figure 2*. In this case, the m^2 profile indicates trapping between the surface and approximately 100 m agl, with another favourable layer for wave propagation from 120 m to 250 m agl approximately. This profile is highly influenced by the dynamical term of the m^2 equation, since the wind direction changes a lot from surface (from SE) to 100 m agl (from NE), and in addition there is a LLJ around 100 m agl. In fact, around 100 m agl, the wind is blowing from NE to SW, while gravity waves are supposedly propagating to E (90º), i.e. they are almost in opposition with wind and the duct layer is not favourable (apart from the influence of the light LLJ). However, we cannot be sure that this height acts as a critical level for wave reflection (ducting from surface to 100 m agl). As said before, GWs parameters are not clear enough to calculate m^2, and therefore, we cannot ensure details about GWs propagation. For this reason, we did not add the m^2 profile to the manuscript. In this new version, we add a paragraph to let the readers know that we cannot say more about propagation with the available data.

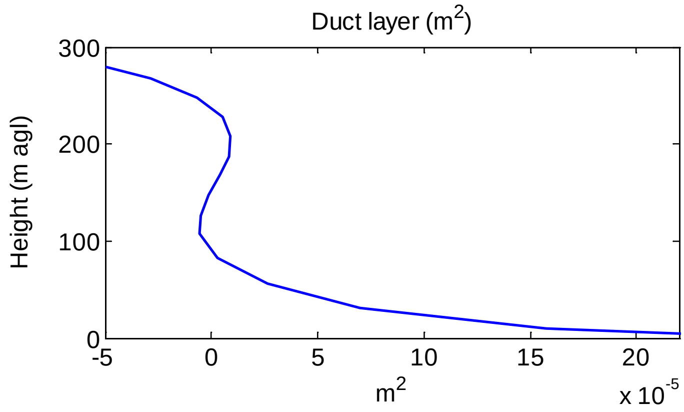

Figure 2*. m^2 calculated with wind and temperature measurements at 19.55 UTC. Positive values indicates favourable duct layer for gravity waves of λ=20 km; c=15 m s^{-1} and phase speed of 15 m s^{-1}

We have the feeling that the layer where GWs can propagate is constantly changing (there is a SDF close to the surface, a LLJ around 100 m agl, then the deeper mountain-plain wind changes the wind profile...). Therefore the GWs features are influenced by these changes (let´s say that the duct layer is changing and affecting the GWs parameters, such as phase speed, wavelength...). In any case, this is just speculation and it cannot be demonstrated with the available data.

3) Figure 8. The profiles of N look quite noisy, while the temperature profile appears relatively smooth. Why? Is this a result of how N is being calculated?

Yes, it is. Reviewer #1 asked the same question and the response is similar for both reviewers.

N_{BV} has been calculated from temperature measurements (potential temperature) at different heights. In fact, the temperature profile shown in Figure 8c is not as smooth as it seems, since it includes narrow unstable layers (and therefore some narrow layers have N_{BV} = 0 s^{-1}). Temperature above 60 m is obtained from measurements of tethered balloon descent, which was averaged **every 5 data** in the first version of the manuscript. However, the heights of these measurements are obtained through GPS and include some uncertainty. These two reasons cause the noisy behaviour of N_{BV} profile. In addition, in two cases, the calculation of these mean values includes several measurements taken at approximately the same height (5 data in the same height). It resulted in uncertain unstable layers at some heights (at 100 m agl for example) (the tethered balloon was stopped for some seconds).

To solve this, a new figure has been prepared (Figure 3*, new Figure 8d), where measurements from tethered balloon are averaged **over 20 m layers** instead of over 5 data points. In this case, N_{BV} profile is smoothed, although it still has a clear layer where N_{BV} becomes 0, located around 200 m agl. We have changed the main text and, according to response to last question (ducting), we state that it is not so easy to determine exactly the layer where GWs are propagating, since it depends on GWs features and wind and temperature profiles. However, we also say that the propagation above 200 m agl is not going to be favoured, since the thermal profile is not stable in a shallow layer at that height.

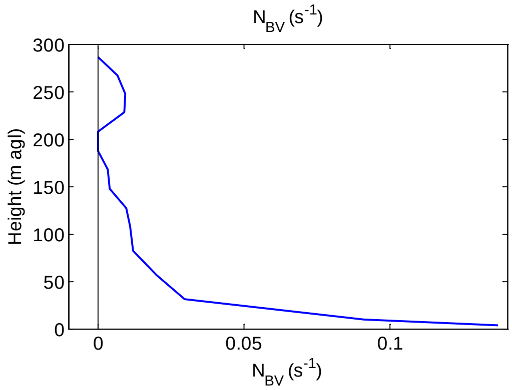

Figure 3*. Brunt-Väisälä frequency (N_{BV}) (s^{-1}) calculated every 20 meters after averaging tethered balloon data.

4) p12834. You may not have measurements of N from the field, but you do have the WRF simulation here. How do the profiles through the deep drainage flow look in the model, and are they consistent with the observed waves during event 2? This may be difficult, depending on how good the model is, but it would be worth checking.

It is indeed a nice suggestion, but maybe this mesoscale model is not appropriate to detect GWs propagation of such characteristics (relatively small wavelengths and periods). Figure 4* shows the evolution of N_{BV} from surface up to 500 m agl from 12.00 to 24.00 UTC of 2nd July. Red colours show N_{BV} > 0.0017 s^{-1} and blue regions N_{BV} < 0.0017 s^{-1}. This frequency is the highest frequency of the detected waves during the whole period (~ 10 minutes of period). It can be observed how these gravity waves (and GWs with larger periods) can exist and propagate in the whole layer from approximately 17.00 UTC onwards. Thus, the model is consistent with the existence of GWs of this type, but maybe it is not appropriate to detect narrow layers with possible ducting.

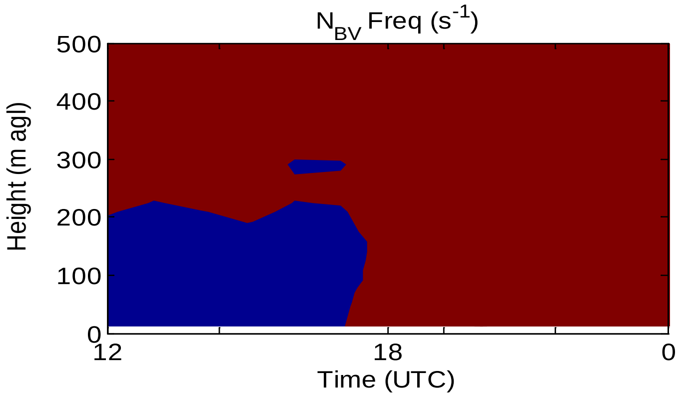

Figure 4*. Brunt Väisäla frequency calculated from potential temperature output of WRF model over Lannemezan. Red colours indicate N_{BV} > 0.0017 s^{-1} and blue colours N_{BV} < 0.0017 s^{-1}. This frequency is the highest frequency of the detected waves during the whole period (~ 10 minutes of period). Thus, red colours indicate regions where the propagation is possible for gravity waves with periods larger than 10 minutes.

5) p12835. Throughout you discuss analysis of the surface fluxes, and plot up friction velocity. A pedantic point perhaps, but friction velocity is not a flux, but (depending on definition – not given in this case) the square root of the absolute value of the momentum flux. There are advantages and disadvantages to using friction velocity rather than the momentum flux. If you decide to stick with friction velocity, then please make sure the text does not imply this is a flux.

We do agree. We have revised completely the text to avoid misunderstandings. We are going to include also the definition of friction velocity (Eq. 1) in the new version of the manuscript:

$$u_* = \left(\left(-\overline{u'w'}\right)^2 + \left(-\overline{v'w'}\right)^2 \right)^{0.25} \qquad \text{Eq. 1}$$

6) p12836. The heat flux values given in the captions of figures 10 and 12 are K m s-1. If this is correct, then these are not heat fluxes, but temperature fluxes. Can you confirm which they are, and ensure the correct term / units are used throughout.

The units are K m s^{-1}, which are indeed temperature fluxes (mean of w’t’) or kinematic heat flux (Stull, 1988, page 48), since we do not include the multiplication by density and c_p. The term has been revised and changed (kinematic heat flux) in the whole text, figures and caption of new version.

7) Section 3.4. There are some intriguing differences here. You mention differences in moisture, but I wonder if the canopy nature of the wheat plays a role here? See for example the literature on nocturnal drainage flows in canopies. I was also interested in the strong differences over the edge site. I do not have a clear enough picture of what the edge site was like to draw real conclusions, but assuming it is hedge like then this perhaps points to the strong impact of features like this on drainage flows, cooling and turbulence in stable boundary layers. In such shallow flows hedges can have an important radiative and thermodynamic impact, as well as a significant dynamical impact on the wind and turbulence. I’ve seen examples of this myself.

We do agree. The differences found between sites are quite surprising and this manifests the important effect of these small heterogeneities of the terrain during SBL and especially during the formation of very shallow and local drainage flows.

In the first version of the manuscript, we wrote “*the heat flux changes from upward to downward considerably later at the Wheat Site than at the other sites. The wheat was drier in this season and therefore the daytime convection is more intensive and the decay takes longer*”. It is true that not only the humidity is involved, the “characteristics of the wheat canopy” can also play a role, since the radiative cooling is hampered by the height of the wheat.

Regarding the second query, it is true that the hedge at the boundary site is influencing the flow (it was a small ditch composed by a different kind of vegetation, although there was a line of three trees close to the boundary tower, see Figures 5a* and 5b*).

Figure 5*. a) Grass tower with line of three trees in the background (to the SE). b) Vegetation composing the boundary site (note that this kind of vegetation is harder than wheat, located in the background). c) Maize field located to the south of the grass site and line of trees at the background (SE). d) Land-use map from van de Boer et al. (2014).

On the other hand, the maize field located to the south (upwind) of the grass site (see Figure 5c* and 5d*), could also be influencing the low wind measured at the grass site. Then, turbulence is increased by collision of the flow with the boundary site and then the flow is different at the wheat.

These considerations have been taken into account and all these hypotheses will be included in the text (Section 3.4), also following recommendations from Reviewer #1.

REF -- Van de Boer, A., Moene, A. F., Graf, A., Schüttemeyer, D., & Simmer, C. (2014). Detection of Entrainment Influences on Surface-Layer Measurements and Extension of Monin–Obukhov Similarity Theory. Boundary-layer meteorology, 152(1), 19-44.

8) The MRFD technique is certainly a nice way of looking at the contributions of different scales to the flow. Do you see some of this scale separation in other techniques, such as more traditional ogive plots?

In fact, MRFD is calculated through the differences between cumulative multi-resolution fluxes for different scales, which is similar to ogive plots. These differences are calculated to obtain the contribution of every range of scales instead of cumulative fluxes. The only difference between ogives and the multi-resolution method (cumulative) is that ogives are calculated using the spectral decomposition of Fourier (sin and cos) and multi-resolution is calculated using the spectral decomposition of Haar basis set. Therefore, we think that the results should be quite similar.

9) I found the conclusions about what eddy covariance averaging time you should use in this case a bit unsatisfactory. It read a bit as if "you should definitely not use an averaging time of more than 60s, so you don't include the wave contributions, unless the wave contributions are wave-generated turbulence, in which case you probably do want to include them." This is not terribly useful for the user who wants to processes their flux data. Can you provide more discussion on this? There is a body of previous work on wave - turbulence interactions, included papers by some of the co-authors. While it is still certainly an open question, placing these findings in the context of other work might be useful. You might want to look at including Durden et al. (2013), Biogeosciences.

We do recognize that our discussion did not provide specific recommendations. However, after long discussions among co-authors, we concluded that we cannot ensure that fluxes contribution from scales larger than 60 s is not turbulent (at least, we have not a common opinion). Any definite conclusions that might come from this site, may not apply to other datasets.

It is true that there is a relatively clear spectral gap around 60 s (see for example Figure 9) and two maxima (one around 5 s (turbulent) and the other centred in larger scales (between 3 and 14 min)). The waves that we detected with the array of microbarometers have periods between 10.5 and 25 minutes, therefore, contributions from periods below these wave periods are not strictly related to the oscillations due to gravity waves. We think that these motions could be caused by transfer of energy from gravity waves to the larger turbulent scales (wave breaking). These potentially turbulent motions are separated (spectral gap) from smaller-scale turbulence generated by other mechanisms (shear, SDF...). This is just a hypothesis and it cannot be demonstrated in the present study. Thus, we are not sure if these motions are non-diffusive (strictly due to gravity waves) or diffusive (turbulent motions but generated by gravity-waves breaking in a chaotic complex atmosphere).

The suggested reference of Durden et al. (2013) presents an interesting case study of influences of gravity waves on fluxes. In this study, the authors concluded that gravity waves are always causing an overestimation of the fluxes (as in Nappo et al. (2008)) if the wave contribution is not removed. We do agree with this theory, however, a question arises when considering periods higher than turbulence but lower than the detected gravity waves. In any case, in our opinion (and in our case study), it is not clear enough if these contributions from scales larger than 60 s are turbulent or not.

We have included this discussion in the conclusion section of the new manuscript, but we include it as an open question, since it could not be demonstrated for our cases. Additionally, we include these two new references (Durden et al. (2013) and Nappo et al. (2008)) along with this discussion.

REF -- Durden, D. J., Nappo, C. J., Leclerc, M. Y., Duarte, H. F., Zhang, G., Parker, M. J., and Kurzeja, R. J.: On the impact of wave-like disturbances on turbulent fluxes and turbulence statistics in nighttime conditions: A case study, Biogeosciences, 10, 8433–8443, doi: 10.5194/bg-10-8433-2013, 2013

REF -- Nappo, C. J., Miller, D. R., and Hiscox, A. L.: Wave-modified flux and plume dispersion in the stable boundary layer, Bound.-Lay. Meteorol., 129, 211–223, 2008.

MINOR / EDITORIAL COMMENTS

10) p12825, lines 1-10. In this discussion of recent work on drainage flows, in might be worth mentioning several significant recent field campaigns (PCAPS - Lareau et al 2013 BAMS, METCRAX - Whiteman et al 2008 BAMS and COLPEX - Price et al, 2011 BAMS) focussing on cold air pooling at different scales and their interaction with other proceses.

The references to these campaigns have been included in this part of the text.

11) p12830, lines 25-28. "Nevertheless, surface heteorgeneities and differences in local slope between BLLAST sites led to differences in thickness and persistence of the SDFs from one location to another (Fig 4), ..."

This sentence has been changed following the suggestion.

12) p12836, line 6. "these contributions ... are clearly separated..." I didn't find this very clear. I don't know if it is the color scheme used in the contour plots, but a number of the features of these MDFD plots were not as obvious to me as the text implied.

We agree that maybe it is not so obvious looking at the MRFD plot and we give an approximate description (in order not to add more plots). What we want to highlight is that there is a maximum centred in turbulent scales (around 2 s) and the other centred in larger scales (around 300 s). In the middle, there is a minimum (spectral gap), which is located around 20 s. It is true that this gap is fluctuating (between 10-60 s). Figure 6* shows the MRFD averaged for the period from 2000 UTC to 2130 UTC. In this graphic, this spectral gap is observed around 20 s (note that this figure is showing the same as Figure 9 (MRFD), but calculated for only for the shorter time interval from 2000 UTC to 2130 UTC.

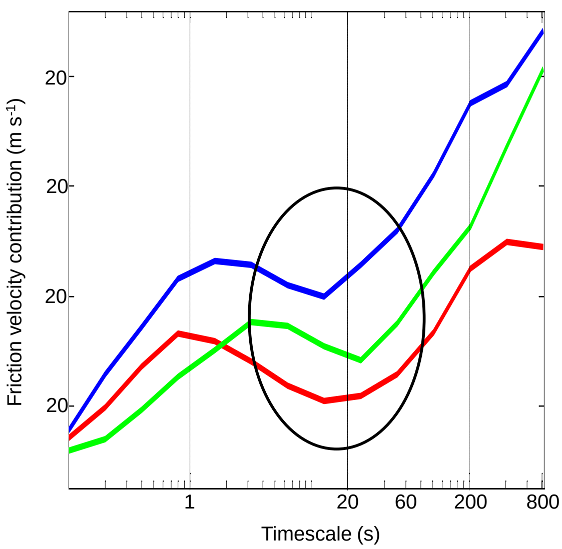

Figure 6*. Friction velocity MRFD (m s^{-1}) averaged for the period comprising from 2000 UTC to 2130 UTC at 0.8 (blue), 2 (red) and 8 m (green) agl. The spectral gap is highlighted with a black ellipse.

13) p12836, line 23. ".. as a consequence of the increase..."

This sentence has been changed following the suggestion.

14) p12838, line 3. "Again, the selection of a larger averaging window..."

This sentence has been changed following the suggestion.

15) p12838, line 14. The phrases "a different kind of vegetation" is not very helpful. Please include a better description of this edge site since this is rather important in interpreting the results. Is it a hedge? Trees? What height? How dense?

It was a small ditch composed by denser vegetation (harder), although there was a line of three trees close to the boundary tower (see Figures 5a and 5b).

16) p12840, lines 22-24. I didn't understand this sentence. How does an increase in mechanical turbulence related to a reduction of large eddies above? Is it not perhaps that the increased mechanical turbulence leads to a reduce temperature gradient and hence a reduced heat flux?

Yes, it is. The sentence was not correctly expressed and it has been changed following the suggestion.

17) p12842, line 16. "MRFD" not "MRDF"?

It has been changed.

18) Figure 3. The caption does not say where these profiles were taken. Also, I would mark on the data points with a symbol so it is clear at which heights the observations are taken rather than just plotting a solid line.

This information has been included in the caption. Profiles are calculated with measurements from the divergence site tower (below 8 m) and from the 60 m tower. Marks have been added to the lines.

19) Figure 5. Again, the caption does not say where this profile is taken.

It has been added. It is over Lannemezan.

20) Figure 6. I found it almost impossible to distinguish the red and purple lines on top of the color contour plot. Perhaps choose a different color, or just stick with solid / dashed lines?

It has been changed in the new version. Now we use a solid red line and dashed black line

21) Figure 8. It is not at all clear from the figure or the text how the measurements at 8 and 60m are integrated in with the tethered balloon profile. Can you plot these as point symbols on these figures? Presumably the line is from the tethered balloon?

In the new figure, we have added marks to the lines (showing where a measurement is taken) and two horizontal lines are included separating the 8m tower, 60m tower and tethered balloon measurements.

22) As a general comment all the figures had rather small labels on the axes / legend which made them hard to read. I would suggest using a larger font size for all these labels.

All the font sizes of axes, labels and legends have been changed.

AUTHORS RESPONSE TO: *Interactive comment on "Interactions among drainage flows, gravity waves and turbulence: a BLLAST case study" by C. Román-Cascón et al.*

Anonymous Referee #3

Answers are in blue and reviewer comments are in black. Please, note that figures of this document are indicated with * symbol, while figures of the manuscript are linked without this symbol.

The authors documented two wave events, and both are associated with the flow from the mountains in the south. They analyzed the wave and turbulence characteristics and their relationship with a shallow drainage flow. The case analyses here are similar to the ones in Sun et al. (2015, JAS, 72, 1484) with a different dataset. The paper is well organized and clear. The dataset is unique. It seems to me that the authors could say more about connections/interactions between the shallow drainage flow, gravity waves, and turbulence.

We do agree, the case presented by Sun et al. (2015) is very similar to this one, with wave-related oscillations observed in surface meteorological parameters, especially very close to the ground, where the stratification is higher. Regarding a deeper analysis, we think that the main aim of the paper is to show a general overview of all processes and not to focus **deeply** on wave-turbulence interactions. The different stages are very clear in this case study and the processes could be tracked quite well. However, after deep analyses of many parameters at different sites of the BLLAST sites and due to the high heterogeneity of the area (and non-perfect nature of waves), we were not able to obtain more specific conclusions about the connections among processes. This is mainly due to the interactions of these processes with the terrain, which makes the study more and more difficult.

In any case, as a result of the queries from the three reviewers, the authors include a deeper explanation of some of the processes commented through the paper in the new version of the manuscript.

Figures 9-12 show the temporal variation of turbulent fluxes as a function of time scale, but the maximum time-scale was capped below the shortest gravity wave period identified in Table 3.

MRFD figures were mainly included to analyse changes and features of turbulence, but not to perform a deep analysis of GWs frequencies. MRFD is a very nice tool to analyse higher frequencies (turbulence), but it has a limited utility if we want to analyse lower frequencies (see for example Viana et al. (2010, JAS, 67, 3949) for a deeper discussion on this issue). In fact, other methods (as wavelet) are more appropriate to deal with longer periods. For this reason, MRFD was truncated at the temporal scale N=14, which is equal to $2^N * \Delta T$ (= 2^{14} *0.05 = 819.2 s = 13.65 min). Where N has to be an integer and ΔT is the frequency of measurements (0.05 s^{-1}). Thus, the next possible analysis would be N=15, equal to 1638.4 s (= 27.3 min), which is larger than the period of observed GWs. Therefore, we lose the information between 13.65 min and 27.3 min, which is where the periods of observed GWs are. In fact, if we plot MRFD until 27.3 min (N=15), the contour figure is going to interpolate between 13.65 and 27.3 min and the colours in the middle could show something not real in this relatively long interval of periods. For this reason, we preferred to truncate the MRFD in N=14. However, for shorter periods (higher frequencies, turbulence), the obtained resolution is much better and the analysis shows interesting features.

One question I have is the relationship between wave propagation direction and the direction of wind convergence. It looks like the drainage flow for either the early shallow one or the later deep one was from the mountains in the south, which opposes the ambient weak wind from north. Thus, the wind convergence in the approximate north-south direction could lead to the displacement required for the buoyancy wave. However, the wave propagation direction is about 90 deg (either from or toward) as listed in Table 3. Is this common that the wave propagation direction is approximately perpendicular to the wind convergence direction?

We think that convergence can cause propagation towards all the directions from the source, but maybe only some of them are favourable (mainly depending on wind profile) for GWs propagation. It seems reasonable to expect also a propagation perpendicular to the wind convergence. However, we do not have the conviction that GWs were formed by the convergence between these flows. Considering the 4 cycles observed from 1900 UTC to 2030 UTC (see Figure 6 or Figure 7), they were also observed at SS2 (which is approximately 5 km to the south from edge site). However, the local character of SDFs was demonstrated, formed at some places but not effectively at others. Besides this, they were very shallow and consequently, the vertical displacement caused by the crash between SDF and the previous N-NE wind is not expected to be very important (at least in the BLLAST area). However, we do not have a better explanation about the genesis of GWs. We think that maybe the katabatic (deeper one) could be observed some time before near the mountains. The interaction of this flow with the complex orography to the south (southwest) from BLLAST area is another possible explanation, but we cannot ensure anything with the available data.

L. 25 on P. 12831. The deeper wind? Maybe the strong wind over a deep layer?

We do agree. This sentence has been changed.

The last sentence before section 3.2.1. The next two sections.

We do agree. This sentence has been changed.

The second line on P. 12834. It seems to me that the depth of a duct layer decides the depth of the wave layer. I am not sure how the depth relates the amplitude of the pressure perturbations.

This is something previously discussed among co-authors. In some cases (Román-Cascón et al. 2015. QJRMS, DOI: 10.1002/qj.2441), we have observed a relation between a narrowing of the duct layer and changes in period/wavelength (the shallower the duct layer is, the smaller the period of the wave). In fact, maybe an analogy with tsunamis in the sea is possible. When these oceanic waves (with longer periods, longer wavelengths, small amplitudes and high speeds in open sea) arrive to shallower waters close to the coast they transform into waves with shorter periods, shorter wavelengths, higher amplitudes and slower speeds.

We are not sure about the analogy, but we think that the depth of the layer could cause changes in the GWs features, including the amplitude. In any case, this is just a hypothesis and for this reason we write in the text "could be due to ..."

If the reviewer considers it appropriate, we can remove this sentence from the paper, since its information is not strictly necessary.

L. 17 on P. 12835. It is hard to see the lack of turbulence generation the middle (2m?). Maybe the authors can consider showing the momentum and heating fluxes integrated over the relevant time-scales too.

We thought about the possibility of including these type of figures (Figure 1*) in the first version of the manuscript. Figure 1* shows the contribution to the friction velocity from different scales during the SDF stage (average of values from 1900 UTC to 1955 UTC). It is true that in this figure it can be observed better the “lack of turbulence in the middle (2m)”. However we decided not to include these kinds of figures because they are a lot of figures (4 figures of MRFD x 3 subfigures x 4 different stages (well-mixed part, near calm, SDF, katabatic). So, in total there are many figures and all this information is indeed shown and can be inferred from the actual MRFD figures.

In any case, if the reviewer considers it appropriate, we can include some of them in the new version of the paper.

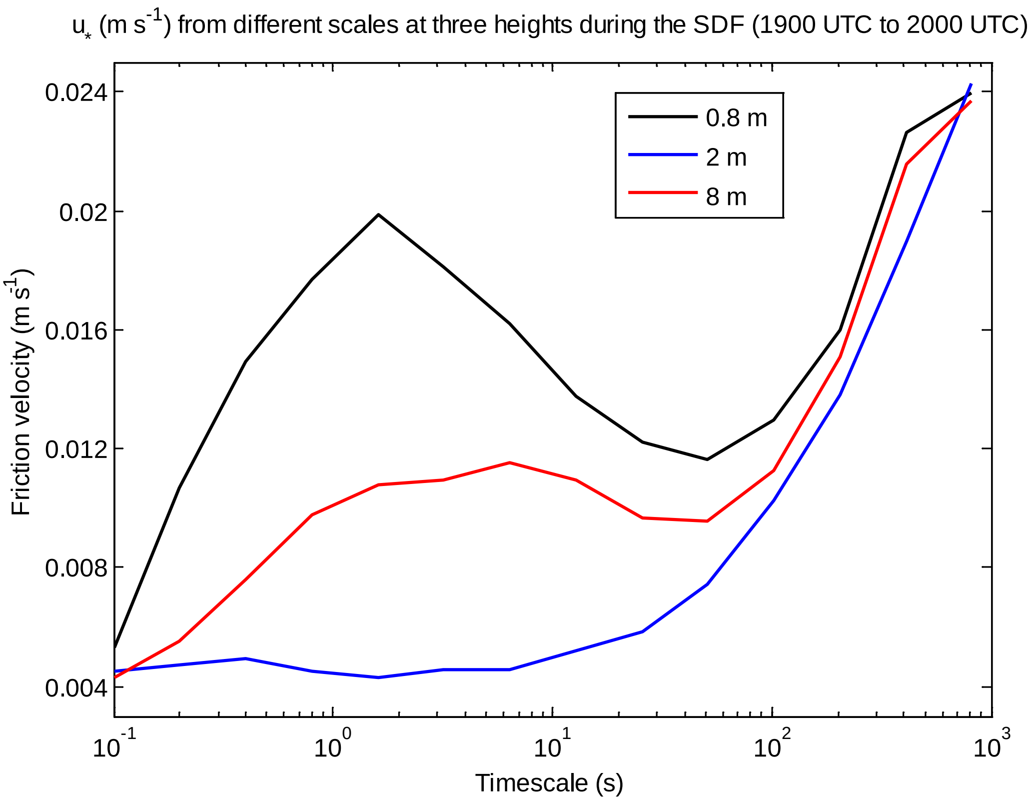

Figure 1*. MRFD of the friction velocity (m s^{-1}) at 0.8 m (black line), 2 m (blue line) and 8 m (red line) at the divergence site from 19.00 UTC to 1955 UTC (SDF stage). Note the lack of turbulence at 2 m, coinciding with the SDF wind maximum.

Table 3. Are the wave propagation directions here the directions waves propagation to or from? The second time period, 2005-2025 UTC, has only one wave cycle if the wave period is 22-24 min. Any justification to divide the wave event 1 into two periods? The wavelet signal of p for this period in Fig.6c could be the signal for wave event 2 extended over depending the size of the window where the wavelet is performed.

They indicate gravity wave propagation (towards). Now, it has been clarified and specified in Table 3.

We think that GWs features of wave event 2 are different from those of wave event 1. In fact, it can be appreciated by looking at Figure 6b. The wavelet signal associated with wave event 1 is centred in periods of 20-25 minutes, while wave event 2 has shorter periods.

The wave events have been divided in two different periods each one (in Table 3) for the calculation of wave parameters. This is done because it is quite difficult to obtain a short range of wave parameters if this calculation is done for relatively long time periods. Therefore, this calculation should be done over short time periods and where the energy of the wavelet is high (see for example Terradellas et al., 2001 or Viana et al., 2009). For this reason, these events have been divided in two. In fact, for the first part (1925 to 2000 UTC) this calculation of wave parameters is not able to provide a clear propagation or clear parameters. On the other hand, it is clearer for the second part (2005 – 2025 UTC).

Figure 1. Since the drainage flow is associated with topography, it would be better to have a topographic map too.

We do agree. We have prepared a new figure (Figure 2*) to be included in the manuscript instead of current Figure 1. Note that we also include the previous image (from Google Earth), since we think that it is also very representative of the heterogeneities in the area.

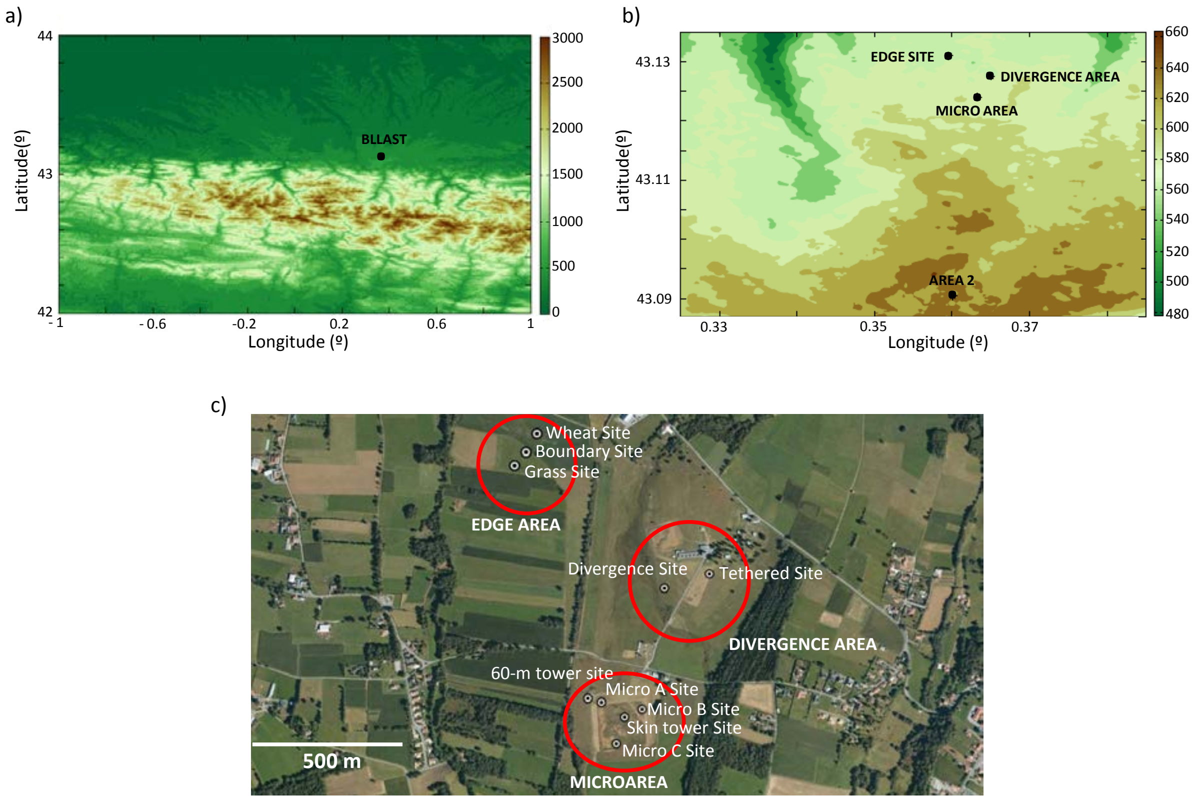

Figure 2* (new Figure 1). a) Topographic map of Pyrenees area around BLLAST. b) Topographic map of BLLAST area. c) Aerial view of BLLAST sites (except Area 2). (NOTE - Figures a and b from Routine ASTER Global Digital Elevation Model from NASA Land Processes Distributed Active Archive Center (LP DAAC). Figure c from Google Earth).

Figure 7. As I understand, Edge area has the lowest elevation, and Area 2 has the highest elevation. However, the pressure at Edge area has the lowest value. This could be real, but different from what I expected.

In fact, the values in brackets in the legend (+4.45 hPa at Area 2 and -3.6 hPa at Edge Area) indicate the value that has been added/subtracted from the original value. That is, at Area 2, 4.45 hPa have been added. However, at the Edge Area, 3.6 hPa have been subtracted from the real values of pressure (for plotting reasons). At the beginning of the plot (1800 UTC), the pressure is of 943.18 – 4.45 = **938.73 at the Area 2** and 943.08 + 3.6 = **946.68 hPa at the Edge Area**. That is, the pressure is higher at the Edge Area (as expected).

Maybe, it was not clear in the legend. In the new version of the manuscript, this is clarified in the figure caption.

Figure 8. Are the sharp changes of wind-speed and direction at 100 m and 200 m real? The temperature profile does not have any signal at these levels.

It seems that there is a slight LLJ around 100 m a.g.l. At 200 m a.g.l., the decrease in wind matches with a narrow unstable layer. The temperature data has now been averaged every 20 meters, following recommendations of reviewer #1 and #2 to obtain a smother N_{BV} profile. This temperature profile indicates also a small unstable layer around 200 m a.g.l, coinciding with the signal obtained in wind at this height. We think that these changes in wind are real.

Manuscript prepared for Atmos. Chem. Phys.
with version 2014/07/29 7.12 Copernicus papers of the LaTeX class copernicus.cls.
Date: 15 July 2015

Interactions among Drainage Flows, Gravity Waves and Turbulence: a BLLAST Case Study

Carlos Román-Cascón[1], Carlos Yagüe[1], Larry Mahrt[2], Mariano Sastre[1], Gert-Jan Steeneveld[3], Eric Pardyjak[4], Anneke van de Boer[3], and Oscar Hartogensis[3]

[1]Dept. de Geofísica y Meteorología. Universidad Complutense de Madrid. Madrid, Spain.
[2]NorthWest Research Associates. Corvallis, OR, USA.
[3]Meteorology and Air Quality Section. Wageningen University. Wageningen, The Netherlands.
[4]Department of Mechanical Engineering. University of Utah. Salt Lake City, UT, USA.

Correspondence to: Carlos Román Cascón (carlosromancascon@ucm.es)

Abstract. The interactions among several stable-boundary-layer (SBL) processes occurring just after the evening transition of 2nd July of 2011 have been analysed using data from instruments deployed over the area of Lannemezan (France) during the Boundary Layer Late Afternoon and Sunset Turbulence (BLLAST) field campaign. The near-calm situation of the afternoon was followed by the formation of local shallow drainage flows (SDFs) of less than ten meters depth at different locations. The SDF stage ended with the arrival of a ~~deeper wind~~ stronger wind over a deeper layer more associated with the mountain-plain circulation, which caused mixing and destruction of the SDFs. Several gravity wave-related oscillations were also observed on different time series. Wavelet analyses and wave parameters were calculated from high resolution and accurate surface pressure data of an array of microbarometers. These waves propagated relatively long distances within the SBL~~, which was confined from the surface to 100 m above ground level~~. The effects of these phenomena on ~~the surface fluxes~~ turbulent parameters (friction velocity and kinematic heat flux) have been studied through Multi Resolution Flux Decomposition methods performed on high frequency data from sonic anemometers deployed at different heights and locations. With this method, we were able to detect the different time-scales involved in ~~surface flux generation~~ each turbulent parameter and separate them from wave contributions, which becomes very important when choosing averaging-windows for surface flux computations using Eddy Covariance methods. The extensive instrumentation allowed us to highlight in detail the peculiarities of the surface ~~fluxes~~ turbulent parameters in the SBL, where several of the noted processes were interacting and producing important variations in ~~the fluxes~~ turbulence with height and ~~among~~ between sites along the sloping terrain.

1 Introduction

A theoretical understanding of stable boundary layers (SBLs) is still an important and unachieved challenge (Mahrt, 2014), especially for numerical weather prediction (NWP) purposes (Van de Wiel et al., 2003; Baklanov et al., 2011; Seaman et al., 2012; Holtslag et al., 2013; Davy and Esau, 2014; Fernando et al., 2015). NWP models have problems representing SBLs (Holtslag et al., 2013; Steeneveld, 2014), which are related, for example, to Planetary Boundary Layer (PBL) evening transitions (Lapworth, 2014), minimum temperatures, low-level winds (Cuxart, 2008) and fog (Van der Velde et al., 2010; Román-Cascón et al., 2012) or air-quality (Andrén, 1990; Baklanov et al., 2009) forecasts. Among the reasons for these difficulties is the existence of the so-called submeso or sub-mesoescale motions (Mahrt, 2009) ~~coexisting~~ that coexist with weak or very weak surface fluxes conditions (Mahrt et al., 2012). These motions (which include wave-like motions in the SBL) do not belong to the mesoscale ~~neither~~ nor to turbulent or micrometeorogical scales. They are usually defined as submeso motions (Mahrt, 2014), comprising scales of less than 2 km, although this limit can be quite subjective. The separation (spectral gap) of these non-turbulent motions from turbulence is not always clear. Therefore, wrong estimations of surface turbulent fluxes are common in SBLs (Vickers and Mahrt, 2003; Voronovich and Kiely, 2007; Viana et al., 2009, 2012), especially over heterogeneous or complex terrain (Martínez et al., 2010; Seaman et al., 2012), where the interactions ~~among~~ between local features and these phenomena complicate the analysis. The processes involved ~~in~~ with the formation of these structures are hard to isolate and the appearance of these motions is often sporadic and ~~not expected~~ unexpected in many cases.

Some small-scale gravity waves (GWs) and drainage flows can be included in the submeso motions; they can significantly change the stable and typical conditions of calm and clear nights through the generation of intermittent turbulence in the SBL (Nappo, 1991; Sun et al., 2002, 2004, 2012; Van de Wiel et al., 2003; Mahrt, 2011, 2014; Vindel and Yagüe, 2011). They can also change the vertical and horizontal gradients of scalars and consequently the turbulent fluxes observed near surface. The theoretical study of these phenomena has been demonstrated to be very complex (Stull, 1988; Sorbjan, 1989; Fernando and Weil, 2010; Mahrt, 2014; Sun et al., 2015b), and some approximations done with laboratory experiments (Hopfinger, 1987; Riley and Lelong, 2000; Ohya et al., 2008) do not include troublesome factors of the real atmosphere. Therefore, the understanding of these processes through the observational analysis of real case studies becomes very important, especially when high-quality micrometeorological data are available for this purpose.

On the one hand, GWs are formed by buoyancy forces when air parcels are vertically displaced from their original equilibrium state (Nappo, 2012). They have been observationally analysed using different approaches (Ralph et al., 1997; Doyle and Durran, 2002; Viana et al., 2009, 2010, 2012; Sun et al., 2012; Román-Cascón et al., 2015d). All these studies illustrate the difficulties in determining the origin and formation mechanisms of GWs, their importance as sources of momentum and heat transport (Sukoriansky et al., 2009; Fernando and Weil, 2010) and the necessity of their accurate parameterization in NWP models (Fritts, 2003; Kim and Hong, 2009; Belušić and Mahrt, 2012; Nappo, 2012; Sun et al., 2015b).

However, detailed analyses of the impact of GWs on ~~turbulent fluxes~~ surface turbulence have received little attention in the literature (Viana et al., 2009; Sun et al., 2015b). In some cases, they have been shown to be structures that are effective at generating intermittent turbulence (Einaudi and Finnigan, 1993; Smedman et al., 1995; Román-Cascón et al., 2015d), while other studies highlight the important turbulence-suppressing effect that they can cause (Viana et al., 2009). In ~~any~~ either case, the ubiquity of GWs in the SBL over a wide variety of scales (Belušić and Mahrt, 2012) and the presence of other turbulent and non-turbulent motions makes the study of these wave-turbulence interactions very complex (Belušić and Mahrt, 2008; Mahrt, 2009). As stated in Sun et al. (2015b), complete understanding of wave-turbulence interactions is an important challenge that ~~remains allusive yet~~ yet remains elusive.

On the other hand, drainage flows are thermal circulations ~~that appear due to~~ generated by the differential cooling between surface air masses in sloped or complex terrain under low synoptic forcing, when local conditions gain importance (Whiteman, 2000; Monti et al., 2002; Soler et al., 2002, 2014; Adachi et al., 2004). They are also typical SBL motions and ~~are manifested~~ manifest as sudden changes in wind direction, a temperature drop (due to the cooler current) or increasing winds at certain heights, among other effects (Yagüe et al., 2006; Viana et al., 2010; Udina et al., 2013). Several field campaigns have recently increased interest in these thermal circulations at different scales: e.g. METCRAX 2006 (Whiteman et al., 2008), COLPEX (Price et al., 2011), PCAPS (Lareau et al., 2013) or METCRAX II (Lehner et al., 2015b).

Drainage flow definitions include a wide range of possible spatial scales (Bossert and Cotton, 1994; Martínez et al., 2010)~~: katabatic~~ . Katabatic and mountain-plain flows are mountain-scale phenomena across and along valleys respectively, while density currents are usually associated with relatively flat terrain. Mountain breezes or katabatic winds (Whiteman, 2000) have been studied in many zones of the world (e.g. Alps (Rotach et al., 2004; Nadeau et al., 2013) or Salt Lake Valley (Doran et al., 2002; Monti et al., 2002)). However, shallow drainage flows (SDFs) or density currents have been less studied ~~in the literature~~ (Mahrt et al., 2001; Soler et al., 2002; Udina et al., 2013; Oldroyd et al., 2014; Lehner et al., 2015a), in part because of their smaller scale, that often makes them more difficult to detect. Their proximity to the surface and their ability to change the surface conditions make them important and interesting phenomena worthy of analysis in SBL studies.

This article deals with a ~~very interesting~~ SBL case study characterized by SDFs generated at different locations just after the near-calm situation of the evening transition during the Boundary Layer Late Afternoon and Sunset Turbulence (BLLAST) field campaign. These SDFs are later broken-up by the arrival of a larger-scale and deeper mountain-plain wind, causing mixing among different layers close to the surface. At the same time, several wave-like oscillations were detected in different time series, related to the passage of GWs. Although these phenomena are common in SBLs, it is not easy to find clear evidence of their existence ~~,~~ given the fine horizontal and vertical resolutions required for such observations. Thus, only a few studies have reported in detail cases like the one here presented, as for example in Sun et al. (2015a).

In this work we try to elucidate the physical mechanisms behind these evening transition processes, which was one of the goals of BLLAST campaign. Moreover, the analysis techniques employed to carry out this study have been shown to be appropriate for performing detailed studies of these local nocturnal-boundary-layer processes. ~~On the one hand~~Firstly, phase differences and wavelet analyses were performed on high-resolution pressure data from an array of microbarometers in order to analyse the detected GWs. ~~On the other hand~~Subsequently, a comparison ~~among~~ of the effects of SDFs, mountain-plain winds and GWs over ~~the surface fluxes~~ surface turbulence have been performed ~~through~~ using Multi Resolution Flux Decomposition (MRFD) methods. The availability of several sonic anemometers at different sites and heights allowed us to explore ~~in detail~~ the spatio-temporal ~~flux behaviour~~ behaviour of turbulence in detail. MRFD is also used to evaluate the relevant scales of turbulence and to separate them from larger-scales, like the observed GWs.

This paper is divided as follows: section 2 explains in detail the BLLAST field campaign, the features and location of the instrumentation and the techniques employed to carry ~~on~~ out the study. Section 3 presents results in several subsections; section 4 summarizes the article and highlights the more important results and conclusions, while also making recommendations for future studies.

2 Data and Methodology

2.1 BLLAST

The BLLAST field campaign (Lothon et al., 2014) took place in Lannemezan (43º 07'N, 0º 21'E, 600 m above sea level (asl)) and its surroundings from 14 June to 8 July 2011. The main objective was to study boundary-layer processes governing the late afternoon transition. The site is located on the plateau of Lannemezan, approximately 40 km North from the Pyrenees main massif, in a quite heterogeneous area (hilly with different land uses). ~~A significant effort was made by numerous international researchers to deploy~~ Numerous international researchers deployed a dense array of meteorological instrumentation. Intense observational periods (IOP) were identified as days with fair weather and weak synoptical forcing. On these days, additional measurements were performed: tethered balloons, aircrafts, unmanned aerial vehicles (UAVs) flights or extra soundings. A total of 12 IOPS resulted from the field campaign. The ~~focus of this paper is~~ paper focuses on a case study corresponding to the 2nd of July 2011 (IOP 10), specifically the period corresponding from approximately 1800 UTC to 2200 UTC. The observation of GWs, shallow flows and mountain-plain winds over these hours makes this day very interesting. Different sites with several research objectives and instrumentation were defined during the BLLAST field campaign around Lannemezan. Figure 1 shows an approximate location of the sites where instrumentation used in the present study was deployed. Table I is a summary with information about these sites and Table II specifies the instruments used at each site. Lothon et al. (2014) include a more detailed description of all these sites.

Drainage flows were mainly investigated at the Divergence Site (additionally at the Micro and Edge Areas), while the GWs analysis from surface pressure records was mainly performed using high-resolution and accurate data from an array of three microbarometers deployed at the Micro Area. Finally, the analysis of ~~turbulent surface fluxes~~ surface turbulent parameters was investigated using data from sonic anemometers installed at different heights on an 8-m tower at the Divergence Site and at the Edge Area, which in turn was composed of three different sites (Wheat Site, Grass Site and the border between these two sites, renamed Boundary Site in this study to avoid confusion).

2.2 Methodology

The relevant physical processes studied in this work have been analysed through the combination of several techniques applied to measurements from different instruments. Initial comparisons were made among time series of atmospheric variables from instrumentation located at several heights and locations. ~~Although simple, it~~ It is instructive to compare the behaviour of these records among sites because they can sometimes suggest some very local processes happening at a certain site but not at another. Moreover, more complex techniques have been applied and explained in the next three subsections.

2.2.1 Wavelet and phase differences analyses

Wavelet transforms are powerful spectral tools for the analysis of time series used in diverse scientific areas, especially in geophysics. In this study, they have been applied to surface pressure time series from three microbarometers. The results are very useful for detecting energy peaks ~~for~~ during specific periods. This analysis can be used ~~as indicator of~~ to identify coherent structures (GWs) when the energy increase remains almost constant for a specific range of periods and during a relatively long time interval. Descriptions of different wavelet transforms are numerous in the literature (Daubechies et al., 1992; Torrence and Compo, 1998). In this work we employ the Morlet wavelet, a complex function consisting of a plane wave modulated by a Gaussian function, (Torrence and Compo, 1998; Cuxart et al., 2002; Viana et al., 2009).

Moreover, wave parameters (wavelength, phase speed and direction of propagation) have been evaluated using phase differences analysis (Terradellas et al., 2001; Viana et al., 2009). This method is based on the time differences observed in the wavelet spectral energy peaks of an atmospheric variable measured at least at three different sites at the surface. In this case, it has been applied over surface pressure time series of three PAROSCIENTIFIC (model 6000-16B) microbarometers (Cuxart et al., 2002), ~~knowing the exact position of them~~with accurately determined positions. These microbarometers were configured in a triangle with a separation of ~~around 150 m among them. They~~

~~operated at a sampling~~ approximately 150m, sampling at a rate of 2 Hz, which allowed a resolution of 0.002 hPa.

2.2.2 Multi-Resolution Flux Decomposition

The Multi-Resolution Flux Decomposition (MRFD) (Howell and Mahrt, 1997; Vickers and Mahrt, 2003) is a multivariate and multiscale statistical tool based on the Haar transform (Haar, 1910). It represents a simple orthogonal decomposition whose spectra satisfy Reynolds averaging at every scale. It has been shown to be a ~~very useful~~ powerful tool for turbulence studies, since it allows the separation of turbulent eddies from possible non-turbulent motions of larger scales when a spectral gap (or minimum of energy of the spectrum) is ~~well defined~~ well-defined (van den Kroonenberg and Bange, 2007; Viana et al., 2009, 2010).

In Section 3.3, MRFD has been applied to time series of different magnitudes (u, v, w for the friction velocity (Eq. 1) and w and ~~T for the heat flux).~~ θ for the kinematic heat flux ($\overline{w'\theta'}$)).

$$u_* = [(-\overline{u'w'})^2 + (-\overline{v'w'})^2]^{0.25} \quad (1)$$

These time series are decomposed into averages of different time scales. The multiresolution coefficients at every step of the sequence are interpreted as contributions to the total flux from the structures of the corresponding time scales. We work with temporal windows ranging from 0 to 13.6 minutes in duration with a one-minute overlap. Finally, a running mean of three minutes is applied over the obtained flux value, in order to smooth the final figures.

2.2.3 WRF model

Although the analysis presented in this study is mainly observational, the Weather Research and Forecasting (WRF-ARW v3.5.1) model has been used as a complement for the determination of the origin of the wind observed at 2030 UTC, since this question could not be resolved solely with the available observational data.

The WRF model is a mesoscale NWP system used for operational and research purposes (Skamarock et al., 2008) which allows the use of several physical parameterizations. In this study, three two-way nested domains centred in Lannemezan (France) were used, with a horizontal resolution of 9, 3 and 1 km respectively and 50 vertically distributed terrain following eta levels. The model was initialized at 0000 UTC of 2$^{\text{nd}}$ July with NCEP-FNL operational global analysis data (1° resolution). It ran for 30 hours (6 hours of spin up) with a time step of 30 s. Yonsei University scheme was used for the PBL parameterization and MM5 similarity for the surface layer scheme. The Noah Land Surface Model was used with input land use and soil category data from USGS. RRTM and Dudhia schemes were selected for the representation of radiation (longwave and shortwave respectively) and the WRF Single-Moment 3-class parameterization was used for the microphysics.

3 Results and discussion

3.1 General analysis

The 2^{nd} of July of 2011 was characterized by a weak surface pressure gradient over the south of France, which led to the predominance of light northerly winds during the afternoon (mixed stage in Figure 2a) and a ~~near calm~~ near-calm period approximately one hour before astronomical sunset, which occurred at 1940 UTC. The wind speed decreased close to the surface around 1855 UTC, with values below 0.5 m s^{-1} at the Divergence Site (Figure 2a, ~~near calm~~ near-calm stage). This site will be the reference site for the SDF analysis due to the availability of six sonic anemometers from 0.8 m to 8 m above ground level (agl). This situation of ~~near calm~~ near-calm is propitious for the appearance of surface drainage flows (SDFs) with a markedly SSE-SE component in the BLLAST area, which is the direction of most of the local slopes where the instrumentation of the field campaign were deployed. These density currents are caused by the differential cooling between near-surface air masses at different locations in sloped terrains. In particular, up to 4 days of the BLLAST field campaign showed SDFs after the near-calm period of the afternoon. The sharp wind direction turning of this case study was well observed around 1855 UTC (Figure 2b) close to the surface, while measurements at higher heights (more than 8 m agl, not shown) indicated a more gradual turning with time until 2000 – 2030 UTC. The wind direction veering near surface was accompanied by a marked wind speed increase. Stronger winds were encountered at lower levels with maxima close to the surface (around 2-3 m agl) and wind intensity decreasing with height. This is the clear picture of a slight SDF blowing from more elevated terrains to lower elevations in a layer close to the ground. The onset of this SDF coincides with the establishment of a surface-based thermal inversion (Figure 2c), although a more ~~intense~~ dramatic decrease in temperature is observed at the lowest levels approximately when the SDF arrives (1840 – 1900 UTC), as is expected when a cold density current appears. This decrease was especially ~~felt~~ noticeable at very low levels (below 1 m agl), which caused the enhancement of the temperature gradient between the ground and higher heights and the correspondent increase of stability close to the surface. The formed SDF was decoupled from the above flow by an upper low-wind layer and by the wind direction differences with height (blue line in Figure 3). Nevertheless, ~~BLLAST sites~~ surface heterogeneities and differences in local slopes ~~led the SDFs to be different~~ between BLLAST sites led to differences in thickness and persistence of the SDFs from one location to ~~other~~ another (Figure 4), even blocking its formation at some places (as Grass and Wheat Sites, both at the Edge Area) where these SDFs were poorly observed or lasted only for a few minutes.

The SDF stage ended between 2000 and 2030 UTC with the arrival of a stronger and deeper wind from SE (Figure 2a and red line in Figure 3, mountain-plain wind stage). This increase in wind was more noticeable at 45 and 60 m agl (not shown) and caused the breaking of the SDF and mixing (increase in temperature) at lower levels (Figure 2c). The WRF model has been used to determine the origin and characteristics of this wind. Results from this mesoscale model simulation indicate that the wind was originated in the southerly located Pyrenees mountains and channelled through the valleys (not shown). The depth of this wind is shown in Figure 5, where maximum in wind speed is observed around 80 m agl. This is a clear indicator of the relatively shallow nature of this flow (compared to winds more related to synoptic scales). Therefore, SDFs were ~~broken~~ disrupted by the arrival of another drainage flow, deeper, stronger and with different characteristics than the former. However, the WRF simulation was neither able to resolve the SDFs nor the GWs observed during these periods.

3.2 Pressure observations

The previously described situation of decoupled layers in the lower PBL ~~is favourable for~~ favours the formation of GWs generated by wind shear in a stable environment. The formation of the SBL around 1800 UTC is characterized by an increase in the wave-like behaviour of the absolute and filtered pressure records from microbarometers (Figure 6a, b). Regarding the filtered pressure, periods greater than 45 minutes have been removed (Figure 6b) using a high-pass Butterworth filter, in order to avoid the pressure tendency and the diurnal cycle.

Two different events can be isolated from the energy increases observed in the wavelet analysis (Figure 6c). The first one corresponds to almost four cycles of 20-25 minutes of period observed during the SDF stage (from 1900 UTC to 2025 UTC approximately, red boxes in Figures 6a-c). The second event is characterized by several oscillations of shorter periods with two notable cycles of greater amplitude from 2030 UTC to 2130 UTC, i.e. after the destruction of the SDF by the arrival of the deeper wind (dashed purple boxes in Figures 6a-c). Wave parameters for these wave-like structures have been evaluated using phase differences analysis (see Section 2.2.1) and are ~~expressed~~ shown in Table III. Both events are analysed in depth in the ~~two~~ next subsections.

3.2.1 Wave event 1 (1900 UTC to 2025 UTC, SDF)

~~The evaluation of wave parameters~~ Wave parameters have been evaluated from phase differences analysis ~~indicates not well defined values for~~ (see Section 2.2.1), knowing the exact position of each microbarometer (Terradellas et al., 2001; Viana et al., 2009). This method is based on the differences between wave phases of the three filtered pressure records (one for each microbarometer). These differences are calculated for a determined time period and attending to different wave periods. Thus, for selected ranges of time and wave periods, we obtain specific ranges of wave parameters. The shorter this range of values is (for example for wavelength), the more monochromatic a wave is. This evaluation indicates that values for the first part of Event 1 ~~(Table III). This means~~ are not well-defined (Table 3, from 1925 to 2000 UTC), meaning that these oscillations are not clear enough due to the superimposition of other structures and motions, which is ~~common in~~ a common feature of the real atmosphere. Only the third cycle (from 2005 to 2025 UTC) shows a shorter range of wave parameters (Table III), indicating clearer wave structures with ~~well defined~~ well-defined parameters: direction of propagation from W towards E, phase speed of around 18 m s^{-1} and approximate wavelength between 23 and 30 km~~approximately~~. On the other hand, all these oscillations (cycles) ~~in~~ of surface pressure were also observed at Area 2 and at the Edge Area (Figure 7), which were located respectively at 3.8 km (to the south) and 1 km (to the north) ~~of distance~~ from the Micro A Site. The resolution and accuracy of the barometers (LICOR barometers, except the microbarometers at Micro Site) located at these sites were not the most appropriate to apply phase differences analysis. However, they were ~~rather useful to affirm~~ used to confirm that these wave-like oscillations were not confined to one specific place and that they were not limited to local SDFs, only observed at some places. ~~Besides this, the terrain altitude differences~~ Additionally, terrain height variance among sites (up to 70 m of difference between Area 2 and Edge Area, see Table I) and the existence of some buildings and forests between sites indicate that the propagation of SDFs was perturbed, while the propagation of the wave-like motions in the pressure signals is clearly observed. With ~~all~~ these outlines, the hypothesis ~~of GWs created~~ that GWs are generated at the top or within the SDF is therefore discarded~~and the idea of propagation~~, while propagation of GWs in a deeper layer ~~gains importance~~becomes more likely.

Figures 8a, b show vertical profiles of both wind speed and ~~direction vertical profiles~~ wind direction obtained from the combination of measurements from the descent of a tethered balloon from 1952 UTC to 1958 UTC and tower measurements at 1955 UTC. These ~~vertical~~ profiles indicate a relatively strong wind shear not only at very shallow levels (as seen before due to the SDF), but also up to 100 m agl, with winds blowing from S-SE at surface and from NE above 50 m agl. Note also the slight LLJ ~~developed~~ around 100 m agl. The Brunt Väisälä (BV) frequency (Figure 8d) has been calculated using temperature data from these sources (Figure 8c) and it shows continuous stable conditions (SBL) up to ~~100 m agl~~approximately 200 m agl. This means that, theoretically, the GWs observed by the microbarometers could propagate from surface up to this height and are trapped in this layer. ~~The~~

It is difficult to explain the physical mechanism leading to the formation of the observed GWs with the available data, therefore, several hypotheses are offered. The first one is the intense wind shear (both in direction and speed of the wind) ~~is the strongest hypothesis we can offer for the formation of these GWs, but other factors~~ between layers in the lowest atmosphere. The convergence of SDFs from S-SE and the previous NE winds or the interaction of these shallow flows with the complex orography in a region located more to the south are other hypotheses for the GWs generation. Besides this, other factors such as the LLJ developed at 100 m agl ~~and the complex orography of the area~~ could also be involved on the GWs generation.

Wave-related oscillations in other surface parameters (wind speed, wind direction and temperature) were also observed at all the locations (see Figures 2 and 4), which indicate the effect of the GWs by alternating horizontal divergence and convergence patterns. Although the agreement between surface pressure and other parameters oscillations is quite good in some cases, linear polarization equations have been not applied to these records because of the existent difficulties when trying to isolate “clean” records in a real atmosphere like the case presented here. These difficulties have also been reported in other works ~~((Nappo, 2012; Mahrt, 2014; Sun et al., 2015b))).~~ (Nappo, 2012; Mahrt, 2014; Sun et al., 2015b).

3.2.2 Wave event 2 (2030 UTC onwards, mountain-plain wind)

Evaluated parameters for the second wave event show differences compared to the first one. In this case, ~~these values do show a short range for the whole event~~ the event is characterised by values with little variation (Table III), especially for the two noteworthy oscillations which caused the highest energy signal observed in the wavelet energy analysis. ~~Unlike in the wave event 1, this fact is indicating~~ This indicates a clear propagation and an absence of perturbations from other motions. These ~~sudden and rapid decreases in surface pressure at 2035 UTC and 2110 UTC are followed by subsequent increases, and they coincide with two observed increases in wind speed (Figure 2a). The surface pressure~~ surface pressure oscillations were also observed at sites separated more than 4 km (Figure 7), which also gives an idea of their horizontal propagation.

The higher amplitudes observed in the surface pressure compared to ~~the wave-event~~ wave event 1 could be due to changes in the depth of the duct layer or stable layer where the GWs were propagating (Román-Cascón et al., 2015d) (see also comment in Román-Cascón et al. (2015c)). That is, the Brunt-Väisälä frequency vertical profile at this stage is ~~surely~~ likely different than the one shown in Figure 8 (at 1955 UTC), but this fact could not be checked due to the unavailability of tethered balloon or radio-sounding data after 2000 UTC.

~~Related oscillations of~~ The oscillations observed in surface pressure from 2035 UTC onwards are related to oscillations in other parameters, such as wind speed (Figure 2a), wind direction (Figure 2b) or temperature (Figure 2c). The wind during this stage is characterised by a wave-like behaviour related to the passage of the GWs, as is observed when compared to filtered surface pressure records (dotted black line in Figure 2a and 2b). Although the oscillations in wind speed have approximately the same period as the oscillations in pressure, the agreement between maxima and minima of both variables is not constant, while the turning of wind speed due to the GWs is more obvious. In this case, maxima in surface pressure coincides with turnings of wind to the south and minima in pressure with turnings to the east direction. These oscillations have an approximate amplitude of 30-45º. Regarding temperature close to the surface, oscillations of several degrees of amplitude were also observed ~~in surface temperature~~ at different heights and sites (see for example Figure 2c at the Divergence site). These oscillations are again ~~quite well~~ moderately correlated to surface pressure, ~~like~~ as in wave event 1. ~~Temperature and wind variations~~ The variations in temperature and wind caused by the GWs at some levels led to a complex evolution of the gradients of these parameters with height, which in turn becomes very important for the surface fluxes and turbulence close to the surface, analysed in the next section.

3.3 Surface ~~fluxes~~turbulence: height differences

The dependence of ~~surface fluxes~~ turbulent parameters on height has been analysed using sonic anemometers at three heights (0.80, 2 and 8 m agl) installed in an 8-m tower at the Divergence Site. Large differences were observed in wind and temperature records between near-ground and upper levels (Figure 2) during the studied period due to the microscale and local behaviour of the SDFs observed at some locations. The ~~surface fluxes were consequently~~ turbulent parameters were affected by these differences and the general evolution ~~of them~~ shows several peculiarities which are analysed hereinafter through MRFD techniques.

For a ~~rapid and~~ clearer interpretation of Figures 9 to 12, one must keep in mind that the x-axis shows the time in UTC and vertical axis indicates ~~the involved~~ temporal scales, while the colorbar shows the magnitude of the ~~turbulent parameter (~~friction velocity or ~~heat flux)~~kinematic heat flux. Therefore, colours indicate the contribution of different temporal scales to the total ~~flux.~~ value of each turbulent parameter.

3.3.1 Friction velocity

A wide range of temporal scales ~~were contributing~~ contributed to the friction velocity (Figure 9) during the mixed stage (until 1830 UTC approximately). However, the smallest scales (below 1 s) were more predominant at 0.8 m agl than at 8 m agl, due to the effect of the surface ground generating very small eddies. Moreover, larger scale eddies (from 10 s to 800 s) were more relevant at 2 and 8 m agl.

The near-calm stage was especially noticeable at the lowest level (0.8 m agl), where a decrease for time scales below 200 s is clearly observed (around 1845 UTC), as a consequence of the decrease in wind and stabilization of the layers very close to the ground. There is still ~~observed a~~ an observed peak for contributions from larger scales (more than 300 s), which is probably the result of larger eddies from the residual layer still present above.

The formation of the SDF after the near-calm stage (around 1900 UTC) enhanced the turbulence very close to the surface (0.8 m agl). However, friction velocity values remained very low for almost all scales at 2 m agl (SDF maximum of wind), while some turbulence is observed at 8 m agl. This ~~is indicating~~ indicates the generation of turbulence by the SDF very close to the ground and above the shallow flow, but not in the middle of the flow (see also comment on Román-Cascón et al. (2015c)). This is the result of the SDF wind profile (Figure 3), with maximum around 2-3 m agl and with wind speed shear vanishing right at this maximum.

A wave-like pattern is also observed in the evolution at this stage, i.e. the friction velocity MRFD analysis shows alternating increases and decreases for scales between 0.5 and 20 s, especially at

0.8 m agl (Figure 9a). This pattern is associated with the GWs-related oscillations seen in the wind speed time series.

The SDF wind shear from 2 to 8 m agl disappeared around 2000 UTC, when wind speed at all levels converged to the same value. This is translated to an increase in the friction velocity at 2 m agl, where the minimum was observed during the previous SDF stage. The decrease in wind shear above 2 m agl ~~caused also the~~ also caused an observed decrease in turbulence at 8 m agl around 2000 UTC. Later on, the arrival of the mountain-plain wind caused the complete destruction of the SDF and the wind shear at low levels decreased considerably. In this case, the mountain-plain wind generated turbulence more effectively at all levels, without the clear minimum observed in the SDF stage.

Contributions to the friction velocity from larger scales are also observed from 1930 UTC onwards, associated with the GWs analysed in Section 3.2.1. In this case, ~~these~~ contributions from 60 to 800 s are ~~clearly~~ separated from smaller scale turbulence (around 2s) by ~~a spectral gap well defined~~ the spectral gap at 20-60 s approximately. That is, the absence of a continuous signal in the MRFD indicates that these contributions to the friction velocity are due to different mechanisms. Since wave-scales are not supposed to contribute significantly to the turbulent mixing, these scales should not be included in a total flux calculation and an averaging window of no more than 20-60 s should be used during this period. However, there is still an open question about the possibility that some of these contributions to the friction velocity from scales between 60 to 800 s are in fact also turbulence, but are generated by the GWs themselves, in which case, they should be included in a total turbulent flux calculation. In any case, the conclusions obtained from this case study and from this dataset should not be applied to other datasets, due to the complexity of the studied event and local features (see comment in Román-Cascón et al. (2015b)).

3.3.2 ~~Heat Flux~~

~~The first difference regarding the surface~~

3.3.2 Kinematic heat Flux

Kinematic heat flux at different heights (Figure 10) ~~is the time when the heat flux changes its sign,~~ changes from upwards to downwards at different times. This change happens first at the lower level and then more than half an hour later at 8 m agl, as result of the progressive stabilization of the layers ~~from ground~~upwards from the surface. After this moment (and already with negative fluxes), there is an increase in the negative fluxes observed at 1815 UTC, especially at 0.8 and 2 m agl and of scales between 1 and 100 s (green colours in Figures 10a and b), as a consequence of the increase in the temperature gradient of the low levels. Later on, the kinematic heat flux magnitude decreases again (yellow colours in Figure 10), which is directly related to the strong decrease in wind speed during the near-calm period.

The SDF stage is characterized by an increase in the contribution of small scales (around 1 s) to the surface kinematic heat flux very close to the ground (at 0.80 m agl, green and blue colours in Figure 10a from 1900 UTC to 2000 UTC) due to the SDF-related increase in friction velocity seen in the previous section. However, at 2 and 8 m agl, this stage is characterized by very low kinematic heat fluxes (near 0, orange colours) because both temperature and wind gradients are smaller at these heights.

Considering the height of 0.8 m agl (Figure 10a), it should be noted ~~the smaller~~ that the temporal scales (around 1s) contributing to the turbulence in this SDF period are smaller when compared to the scales observed before the arrival of the density current. The mean wind speed at 0.8 m agl (not shown) was of approximately 1 m s^{-1} from 1800 UTC to 1830 UTC and of 1.5 m s^{-1} during the SDF stage (1900 UTC to 2030 UTC). If we apply the frozen eddies hypothesis of Taylor (Stull, 1988) to convert temporal scales to length scales for both periods, we obtain approximate eddy sizes of 5 m and 1.5 m respectively~~for both periods~~. In fact, the turbulence generated near surface due to the SDF is observed only in the lowest levels, but not at higher levels, while during the period previous to the near-calm situation (1800 UTC to 1830 UTC), this increase in turbulence was also observed at 2 m agl and up to 5 m agl (not shown). The same can be concluded from friction velocity MRFD (Figure 9) and it is indicative of the small eddies generated by the SDF by friction with the ground compared to the predominant eddies during low-winds-stable situations (period previous to the ~~near calm~~ near-calm situation).

Finally, the arrival of the mountain-plain wind causes an increase in temperature at all levels except 8 m agl (Figure 2c), meaning that the wind is causing mixing among the lowest levels and breaking the SDF. That is, air from aloft is brought to lower levels and therefore the temperature increases, but this increase is progressive with height; it takes place sooner and it is more pronounced at higher heights, enhancing the temperature gradient between levels located very close to the ground. This fact and the increase in wind lead to an enhancement of the negative surface kinematic heat fluxes at 0.8 m agl (blue colours in Figure 10a) at 2015 UTC. However, the mixing at the highest level (8 m agl) causes the homogenization of the layer and therefore the heat flux does not increase (Figure 10c) at 8 m agl. Later on, several increases and decreases in the heat flux are observed (especially at 0.80 m agl), corresponding to the wave-like behaviour of this period. As seen in the friction velocity MRFD, the turbulent scales are well separated from non-turbulent motions by a spectral gap around 10 s. Again, the ~~election~~ selection of a higher averaging window could cause an overestimation of the fluxes, since large scales could be associated with GWs.

3.4 Surface ~~fluxes~~turbulence: site differences

The difficulties estimating surface fluxes over heterogeneous terrain are well known, especially during very stable situations. In this section we compare the evolution of ~~turbulence~~ turbulent parameters through MRFD performed over measurements of three nearby sonic anemometers located at the so-called Edge Area. These instruments were strategically deployed on different land use sites and separated around 60 m among them, allowing us to analyse the effect of the different roughness lengths ~~over the surface fluxes~~and land use over surface turbulence. These sonic anemometers were installed at 2 m agl over grass (10 cm height approximately), wheat (80 cm height approximately) and over the border between them~~, which~~. This border (boundary site) was composed by ~~a different kind of vegetation~~ denser vegetation (harder) and a small ditch (see van de Boer et al. (2014) and comment on Román-Cascón et al. (2015b) for more information and figures about the Edge Area).

3.4.1 Friction velocity

The near-calm period is observed at all the places some minutes before 1900 UTC but with slight differences in the starting time (Figure 11). The SDF was not effectively formed at the Edge Area (see Figure 4a, b), and therefore, a clear related increase in surface turbulence was neither observed at the Grass Site, nor at the Wheat Site. However, certain increase in turbulence is observed at the boundary between these places (Figure 11c from 1900 to 1945 UTC) and reveals the turbulence enhancement effect of this border.

The wind records at the Grass Site were clearly characterized by a wave-like behaviour during this stage ~~and a maximum is~~ with a maximum observed at the lowest levels (less than 5 m agl) around 1930 UTC, which indicates an attempt of settling of some SDF (see Figure 4a). This increase in wind does not cause a direct increase in mechanical turbulence at the Grass Site (Figure 11a), but it does it over the Boundary Site (Figure 11c). This increase is possibly a consequence of the crash between a ~~very~~ shallow flow from SE (from Grass Site) and the denser and higher vegetation at ~~this~~ the Boundary Site. Beyond this point (at the Wheat Site) this increase is again not observed, except for very small scales (below 1s). This fact is contrary to the processes observed at the Grass Site, where these small contributions were almost suppressed from 1830 to 2015 UTC, as a result of very small winds observed at the Grass Site during this period. These low winds observed at the Grass Site could be in turn affected by the maize field located upwind (to the south, see comment on Román-Cascón et al. (2015a)).

With the arrival of the mountain-plain wind around 2015 UTC, the turbulence slightly increases at the Grass and Wheat ~~Sites~~Site, while there is a marked increase at the Boundary Site (Figure ~~10c~~11c), highlighting again the important effect of this obstacle between both places generating turbulence. In this stage, the very small-scale turbulence increase was observed at both sites, although it is more noticeable at the Wheat Site. The important increase in wind observed at the Grass Site some minutes before 2030 UTC (Figure 4a) is the cause of this enhancement ~~of~~ observed in the friction velocity MRFD. However, reasons for the specific scale-contributions in this case are difficult to determine and are probably related to the roughness length of the different surfaces. It seems that unlike in the SDF stage, the grass roughness is acting efficiently in the generation of turbulence, mainly because of the important increase ~~observed~~ in wind speed observed at 2 m agl at 2025 UTC (Figure 4a), where the wind changes radically with the arrival of the mountain-plain wind.

Finally, the effects of the observed GWs are also present at all the sites, with important large-scale contributions for scales higher than 100 s and especially for scales of the order of minutes, as seen also before at the Divergence Site (Figure 9). However, the GWs effects are not only observed over these large-scale contributions; there is a clear wave-like behaviour in turbulent scales (intermittent turbulence) during the whole period, with maximum followed by minimum contributions for all the involved scales. This is the result of the alternating horizontal divergence and convergence patterns of the SBL caused by the waves. That is, the oscillations observed in temperature and wind profiles at different heights are causing alternating increases and decreases in the temperature and wind gradients, which is consequently translated into these changes in surface fluxes.

3.4.2 ~~Heat~~ Kinematic heat Flux

Large differences have also been found among surface kinematic heat fluxes analysed at these three nearby but different places (Figure 12). It is interesting to note that the kinematic heat flux changes from upward to downward considerably later at the Wheat Site than at the other sites. The wheat was drier in this season and therefore the daytime convection is more intensive and the decay takes longer. Consequently, the increase in negative surface kinematic fluxes due to the stabilization of the layer around 1800 UTC at the other sites is not observed at the Wheat Site. The characteristics of the wheat canopy could also play a role limiting the effect of the radiative cooling by the wheat itself.

The near-calm period just before 1900 UTC is well observed at all ~~the places~~sites, especially at the Grass Site, ~~were~~ where the diffusion of heat was almost completely suppressed for all scales. Later on, during the SDF stage, there is a tendency ~~to find very small~~ toward very small kinematic heat fluxes over wheat and grass surfaces (yellow colours), while an increase in the negative heat fluxes is observed at the edge between the ~~places~~ sites (Boundary Site, Figure 12c), as also seen and explained in the previous section (greater friction velocity).

The consequences of the arrival of the mountain-plain wind are also very different depending on the site. Contrary to expected, a reduction of the surface fluxes is observed when the wind increases, and only small scales are contributing to diffuse the heat downward at the Grass Site (yellow colour below 3 s versus orange colour for contributions between 3 to 60 s, from 2015 UTC onwards). Although the mechanical turbulence slightly increased at this time (Figure 11 at 2015 UTC), the kinematic heat flux drop ~~is~~ was probably caused by the mixing that occurred at higher levels, leading to a reduction of ~~larger eddies above~~the temperature gradient. In contrast, the effect of the mountain-plain wind over the Wheat site was to cause the enhancement of the negative kinematic heat fluxes, ~~whose explanation~~ the explanation of which is hard to determine, since the temperature gradient behaviour was similar at the Grass Site (not shown).

The gap between turbulent and larger scales is very ~~well defined~~ well-defined at these sites during the whole period. There are clear alternations between positive and negative values (red and blue colours) of large scales, which is a distinctive characteristic of GWs (Viana et al., 2009, 2010). The spectral gap is especially well marked at the Boundary Site (Figure 12c), where a change from negative (turbulence) to positive contributions (probably related to waves) is observed around 60 s from 1900 UTC onwards. In this case, an inappropriate choice of the averaging interval when using eddy covariance methods to estimate turbulent ~~heat fluxes~~ parameters could lead to an important underestimation or even be the cause of the counter-gradient fluxes found sometimes in SBLs.

4 Summary and conclusions

Several stable-boundary-layer processes occurring along the afternoon and evening transition during the 2$^{\text{nd}}$ of July 2011 (IOP 10) of the BLLAST field campaign have been analysed in detail taking advantage of the large amount of accurate and high frequency instrumentation deployed over the area of Lannemezan (France).

Shallow drainage flows (SDFs) were formed just after the near-calm period of the afternoon at different locations due to small local slopes. The formation of these density currents led to untypical wind profiles, with maxima in wind speed around 2-3 m agl, decreasing winds with height and marked changes in wind direction among different levels. These SDFs (not observed at all the sites due to heterogeneities of the area) were eroded by the arrival of a mountain-plain wind. This deeper wind was more associated with the scale of the Pyrenees and caused partial mixing and the establishment of new wind and temperature profiles.

Time series of pressure, wind and temperature showed a wave-like pattern during the SDFs stage and during the mountain-plain wind. The availability of precise and high-frequency data of surface pressure from an array of microbarometers allowed us to evaluate wave parameters, which indicated a shorter (more precise) range of values for gravity waves (GWs) parameters during the mountain-plain wind, with smaller wavelengths and phase speeds. These GWs were observed at different locations, indicating a non-local character and a clear propagation. Tethered balloons and tower measurements indicated stable stratification ~~up to 100~~ at least up to 200 m agl, wind direction changing with height and even a weak LLJ ~~at the top of the SBL~~around 100 m agl. This wind shear or even the LLJ effects are proposed to be involved in the generation of these GWs, which in any case were trapped within the SBL. However, the effect of the nearby hilly terrain could also be important.

Finally, the effects of these different processes on the surface ~~fluxes~~ turbulent parameters (friction velocity and kinematic sensible heat flux) have been studied in detail using Multi Resolution Flux Decomposition (MRFD) techniques from sonic anemometers data installed at different heights and sites. The microscale and shallow nature of some of these processes is underscored ~~through~~ by the differences found at several heights. The selection of the height of the sensor could lead to underestimations of surface fluxes or turbulent parameters when density currents are present in very shallow layers, specially if sonic anemometers are located at the SDF wind-maximum height (minimum in turbulence). The dependence of these ~~fluxes~~ turbulent parameters on the land-use and terrain is also highlighted through the comparison among the ~~MRDF~~ MRFD at the grass, wheat and at the boundary between both sites.

MRFD is shown to be a powerful tool to determine the averaging-window needed to compute turbulent parameters or fluxes from the spectral gap observed between ~~turbulence~~ turbulent and larger-scale motions, as done in (Nappo et al., 2008; Durden et al., 2013), where GWs scales are removed from the flux computation in order to avoid overestimation of fluxes. Otherwise, possibly wrong estimations of momentum (overestimation) and heat (overestimation, underestimation or even false counter-gradient) turbulent fluxes can be assumed. ~~Although~~ However, there is still an open question about the possible overlapping between wave scales and wave-generated turbulence (separated by a spectral gap from turbulence of smaller scales created by other mechanisms). In this case, part of these larger scales should be definitely included (Vercauteren and Klein, 2014), since their turbulent behaviour would contribute to the diffusion of scalars. These considerations ~~have to~~ must be taken into account, especially when analysing SBLs over heterogeneous terrain and during the evaluation of numerical models performance with field measurements.

Acknowledgements. This research has been funded by the Spanish Government (projects CGL2009-12797-C03-03, CGL2011-13477-E and CGL2012-37416-C04-02). BLLAST field experiment was made possible thanks to the contribution of several institutions and supports: INSU-CNRS (Institut National des Sciences de l'Univers, Centre national de la Recherche Scientifique, LEFE-IDAO program), Météo-France, Observatoire Midi-Pyrénées (University of Toulouse), EUFAR (EUropean Facility for Airborne Research) and COST ES0802 (European Cooperation in the field of Scientific and Technical). The field experiment would not have occurred without the contribution of all participating European and American research groups, which all have contributed ~~in a significant amount~~significantly. BLLAST field experiment was hosted by the instrumented site of Centre de Recherches Atmosphériques, Lannemezan, France (Observatoire Midi-Pyrénées, Laboratoire d'Aérologie). BLLAST data are managed by SEDOO, from Observatoire Midi-Pyrénées. The tower equipment ~~has been~~ was supported by CNRS, University of Toulouse and European POCTEFA FluxPyr program and FEDER program (Contract 34172 – IRENEA – ESPOIR). Corn and Moor stations were funded by the CNRS INSU and Météo-France and implemented by the CNRM-GAME team GMEI/4M. The Edge Site measurements were financed by the DFG (Deutsche Forschungsgemeinschaft) project GR2687/3-1 and SCHU2350/2-1. Gert-Jan Steeneveld contribution was supported by the NWO-VENI grant 863.10.010.

References

Adachi, A., Clark, W. L., Hartten, L. M., Gage, K. S., and Kobayashi, T.: An observational study of a shallow gravity current triggered by katabatic flow, Ann. Geophys., 22, 3937–3950, doi:10.5194/angeo-22-3937-2004, 2004.

Andrén, A.: Evaluation of a turbulence closure scheme suitable for air-pollution applications, Journal of applied meteorology, 29, 224–239, 1990.

Baklanov, A. A., Grimmond, S., Mahura, A., and Athanassiadou, M.: Meteorological and Air Quality Models for Urban Areas, Springer. 140 pp., 2009.

Baklanov, A. A., Grisogono, B., Bornstein, R., Mahrt, L., Zilitinkevich, S. S., Taylor, P., Larsen, S. E., Rotach, M. W., and Fernando, H.: The nature, theory, and modeling of atmospheric planetary boundary layers, Bull. Am. Meteorol. Soc., 92, 123–128, 2011.

Belušić, D. and Mahrt, L.: Is geometry more universal than physics in atmospheric boundary layer flow?, Journal of Geophysical Research: Atmospheres (1984–2012), 117, 2012.

Belušić, D. and Mahrt, L.: Estimation of length scales from mesoscale networks, Tellus, A, 60, 706–715, doi:10.1111/j.1600-0870.2008.00328.x, 2008.

Bossert, J. E. and Cotton, W. R.: Regional-scale flows in mountainous terrain. Part 1: A numerical and observational comparison, Mon. Weather Rev., 122, 1449–1471, doi:10.1175/1520-0493(1994)122<1449:RSFIMT>2.0.CO;2, 1994.

Cuxart, J.: Nocturnal basin low-level jets: an integrated study, Acta Geophys., 56, 100–113, doi:10.2478/s11600-007-0042-2, 2008.

Cuxart, J., Morales, G., Terradellas, E., and Yagüe, C.: Study of coherent structures and estimation of the pressure transport terms for the nocturnal stable boundary layer, Boundary-Layer Meteorol., 105, 305–328, doi:10.1023/A:1019974021434, 2002.

Daubechies, I. et al.: Ten lectures on wavelets, vol. 61, Society for Industrial and Applied Mathematics (SIAM). Capital City Press. Philadelphia. 354 pp., 1992.

Davy, R. and Esau, I.: Global climate models' bias in surface temperature trends and variability, Environ. Res. Lett., 9, 114 024, doi:10.1088/1748-9326/9/11/114024, http://dx.DOI.org/10.1088/1748-9326/9/11/114024, 2014.

Doran, J. C., Fast, J. D., and Horel, J.: The VTMX 2000 campaign, Bull. Am. Meteorol. Soc., 83, 537–551, doi:10.1175/1520-0477(2002)083<0537:TVC>2.3.CO;2, 2002.

Doyle, J. D. and Durran, D. R.: The Dynamics of Mountain-Wave-Induced Rotors, J. Atmos. Sci., 59, 186–201, doi:10.1175/1520-0469(2002)059<0186:TDOMWI>2.0.CO;2, 2002.

Durden, D., Nappo, C., Leclerc, M., Duarte, H., Zhang, G., Parker, M., and Kurzeja, R.: On the impact of wave-like disturbances on turbulent fluxes and turbulence statistics in nighttime conditions: a case study, Biogeosciences, 10, 8433–8443, 2013.

Einaudi, F. and Finnigan, J. J.: Wave-turbulence dynamics in the stably stratifies boundary layer, J. Atmos. Sci., 50, 1841–1864, doi:10.1175/1520-0469(1993)050<1841:WTDITS>2.0.CO;2, 1993.

Fernando, H., Pardyjak, E., Sabatino, S. D., Chow, F., Wekker, S. D., Hoch, S., Hacker, J., Pace, J., Pratt, T., Pu, Z., Steenburgh, W., Whiteman, C., Wang, Y., Zajic, D., Balsley, B., Dimitrova, R., Emmitt, G., Higgins, C., Hunt, J., Knievel, J., Lawrence, D., Liu, Y., Nadeau, D., Kit, E., Blomquist, B., Conry., P., Coppersmith, R., Creegan, E., Felton, M., Grachev, A., Gunawardena, N., Hang, C., Hocut, C., Huynh, G., Jeglum, M., Jensen, D., Kulandaivelu, V., Lehner, M., Leo, L., Liberzon, D., Massey, J., McEnerney, K., Pal, S., Price, T., Sghiatti, M., Silver, Z., Thompson, M., Zhang, H., and Zsedrovits, T.: THE MATERHORN - Unraveling the Intricacies of Mountain Weather, To be submitted to Bull. Am. Meteorol. Soc., 2015.

Fernando, H. J. S. and Weil, J. C.: Whither the stable boundary layer?, Bull. Am. Meteorol. Soc., 91, 1475–1484, doi:10.1175/2010BAMS2770.1, 2010.

Fritts, D. C.: Gravity wave dynamics and effects in the middle atmosphere, Rev. Geophys., 41, 1003, doi:10.1029/2001RG000106, http://DOI.wiley.com/10.1029/2001RG000106, 2003.

Haar, A.: Zur Theorie der orthogonalen Funktionensysteme (On the theory of orthogonal function systems), Math. Ann., 69, 331–371, 1910.

Holtslag, A., Svensson, G., Baas, P., Basu, S., Beare, B., Beljaars, A., Bosveld, F., Cuxart, J., Lindvall, J., Steeneveld, G., et al.: Stable atmospheric boundary layers and diurnal cycles: challenges for weather and climate models, Bull. Am. Meteorol. Soc., 94, 1691–1706, 2013.

Hopfinger, E.: Turbulence in stratified fluids: a review, J. Geophys. Res., 92, 5287–5303, doi:10.1029/JC092iC05p05287., 1987.

Howell, J. and Mahrt, L.: Multiresolution flux decomposition, Boundary-Layer Meteorol., 83, 117–137, doi:10.1023/A:1000210427798, http://link.springer.com/article/10.1023/A:1000210427798, 1997.

Kim, Y. J. and Hong, S. Y.: Interaction between the orography-induced gravity wave drag and boundary layer processes in a global atmospheric model, Geophys. Res. Lett., 36, 19–23, doi:10.1029/2008GL037146, 2009.

Lapworth, A.: Observations of the site dependency of the morning wind and the role of gravity waves in the transitions, Q. J. R. Meteorol. Soc., doi:10.1002/qj.2340, 2014.

Lareau, N. P., Crosman, E., Whiteman, C. D., Horel, J. D., Hoch, S. W., Brown, W. O., and Horst, T. W.: The persistent cold-air pool study, Bull. Am. Meteorol. Soc., 94, 51–63, 2013.

Lehner, M., Whiteman, C., Hoch, S., Jensen, D., Pardyjak, E., Leo, L., Di Sabatino, S., and Fernando, H.: A case study of the nocturnal boundary-layer evolution on a slope at the foot of a desert mountain, J. Appl. Meteorol. Climatol., doi:DOI:10.1175/JAMC-D-14-0223.1, in press, ~~2015.~~ 2015a.

Lehner, M., Whiteman, C. D., Hoch, S. W., Crosman, E. T., Jeglum, M. E., Cherukuru, N. W., Calhoun, R., Adler, B., Kalthoff, N., Rotunno, R., et al.: The METCRAX II field experiment-A study of downslope windstorm-type flows in Arizona's Meteor Crater, Bull. Am. Meteorol. Soc., 2015b.

Lothon, M., Lohou, F., Pino, D., Couvreux, F., Pardyjak, E., Reuder, J., Vilà-Guerau de Arellano, J., Durand, P., Hartogensis, O., Legain, D., others, D., Augustin, P., Gioli, B., Faloona, I., Yagüe, C., Alexander, D. C., Angevine, W. M., Bargain, E., Barrié, J., Bazile, E., Bezombes, Y., Blay-Carreras, E., van de Boer, A., Boichard, J. L., Bourdon, A., Butet, A., Campistron, B., de Coster, O., Cuxart, J., Dabas, A., Darbieu, C., Deboudt, K., Delbarre, H., Derrien, S., Flament, P., Fourmentin, M., Garai, A., Gibert, F., Graf, A., Groebner, J., Guichard, F., Jimenez Cortes, M. A., Jonassen, M., van den Kroonenberg, A., Lenschow, D. H., Magliulo, V., Martin, S., Martinez, D., Mastrorillo, L., Moene, A. F., Molinos, F., Moulin, E., Pietersen, H. P., Piguet, B., Pique, E., Román-Cascón, C., Rufin-Soler, C., Saïd, F., Sastre-Marugán, M., Seity, Y., Steeneveld, G. J., Toscano, P., Traullé, O., Tzanos, D., Wacker, S., Wildmann, N., and Zaldei, A.: The BLLAST field experiment: Boundary-layer late afternoon and sunset turbulence, Atmos. Chem. Phys., 14, 10 931–10 960, 2014.

Mahrt, L.: Characteristics of submeso winds in the stable boundary layer, Boundary-Layer Meteorol., 130, 1–14, doi:10.1007/s10546-008-9336-4, 2009.

Mahrt, L.: Surface wind direction variability, J. Appl. Meteorol. Climatol., 50, 144–152, doi:10.1175/2010JAMC2560.1, 2011.

Mahrt, L.: Stably Stratified Atmospheric Boundary Layers, Annu. Rev. Fluid Mech., 46, 23–45, doi:10.1146/annurev-fluid-010313-141354, http://www.annualreviews.org/DOI/abs/10.1146/annurev-fluid-010313-141354, 2014.

Mahrt, L., Vickers, D., Nakamura, R., Soler, M. R., Sun, J., Burns, S., and Lenschow, D. H.: Shallow drainage flows, Boundary-Layer Meteorol., 101, 243–260, doi:10.1023/A:1019273314378, 2001.

Mahrt, L., Richardson, S., Seaman, N., and Stauffer, D.: Turbulence in the nocturnal boundary layer with light and variable winds, Q. J. R. Meteorol. Soc., 138, 1430–1439, doi:10.1002/qj.1884, 2012.

Martínez, D., Jiménez, M. A., Cuxart, J., and Mahrt, L.: Heterogeneous Nocturnal Cooling in a Large Basin Under Very Stable Conditions, Boundary-Layer Meteorol., 137, 97–113, doi:10.1007/s10546-010-9522-z, 2010.

Monti, P., Fernando, H. J. S., Princevac, M., Chan, W. C., Kowalewski, T. A., and Pardyjak, E. R.: Observations of Flow and Turbulence in the Nocturnal Boundary Layer over a Slope, J. Atmos. Sci., 59, 2513–2534, doi:10.1175/1520-0469(2002)059<2513:OOFATI>2.0.CO;2, 2002.

Nadeau, D. F., Pardyjak, E. R., Higgins, C. W., Huwald, H., and Parlange, M. B.: Flow during the evening transition over steep Alpine slopes, Q. J. R. Meteorol. Soc., 139, 607–624, doi:10.1002/qj.1985, 2013.

Nappo, C., Miller, D., and Hiscox, A.: Wave-modified flux and plume dispersion in the stable boundary layer, Boundary-layer meteorology, 129, 211–223, 2008.

Nappo, C. J.: Sporadic breakdown of stability in the PBL over simple and complex terrain, Boundary-Layer Meteorol., 54, 69–87, doi:10.1007/BF00119413, 1991.

Nappo, C. J.: An introduction to atmospheric gravity waves (2nd ed.), vol. 102, Academic Press, 2012.

Ohya, Y., Nakamura, R., and Uchida, T.: Intermittent bursting of turbulence in a stable boundary layer with low-level jet, Boundary-Layer Meteorol., 126, 349–363, doi:10.1007/s10546-007-9245-y, 2008.

Oldroyd, H. J., Katul, G., Pardyjak, E. R., and Parlange, M. B.: Momentum balance of katabatic flow on steep slopes covered with short vegetation, Geophys. Res. Lett., 41, 4761–4768, doi:DOI:10.1002/2014GL060313, 2014.

Price, J., Vosper, S., Brown, A., Ross, A., Clark, P., Davies, F., Horlacher, V., Claxton, B., McGregor, J., Hoare, J., et al.: COLPEX: field and numerical studies over a region of small hills, Bull. Am. Meteorol. Soc., 92, 1636–1650, 2011.

Ralph, F. M., Neiman, P. J., Keller, T. L., Levinson, D., and Fedor, L.: Observations, Simulations, and Analysis of Nonstationary Trapped Lee Waves, J. Atmos. Sci., 54, 1308–1333, doi:10.1175/1520-0469(1997)054<1308:OSAAON>2.0.CO;2, 1997.

Riley, J. J. and Lelong, M.-P.: Fluid motions in the presence of strong stable stratification, Annu. Rev. Fluid Mech., 32, 613–657, doi:10.1146/annurev.fluid.32.1.613, 2000.

Román-Cascón, C., Yagüe, C., Sastre, M., Maqueda, G., Salamanca, F., and Viana, S.: Observations and WRF simulations of fog events at the Spanish Northern Plateau, Adv. Sci. Res., 8, 11–18, doi:10.5194/asr-8-11-2012, http://www.adv-sci-res.net/8/11/2012/, 2012.

Román-Cascón, C., Yagüe, C., Mahrt, L., Sastre, M., Steeneveld, G., Pardyjak, E., van de Boer, A., and Hartogensis, O.: Comment, Atmos. Chem. Phys. Discuss., 15, C3759–C3759, 2015a.

Román-Cascón, C., Yagüe, C., Mahrt, L., Sastre, M., Steeneveld, G., Pardyjak, E., van de Boer, A., and Hartogensis, O.: Comment, Atmos. Chem. Phys. Discuss., 15, C3760–C3760, 2015b.

Román-Cascón, C., Yagüe, C., Mahrt, L., Sastre, M., Steeneveld, G., Pardyjak, E., van de Boer, A., and Hartogensis, O.: Comment, Atmos. Chem. Phys. Discuss., 15, C3761–C3761, 2015c.

Román-Cascón, C., Yagüe, C., Viana, S., Sastre, M., Maqueda, G., Lothon, M., and Gomara, I.: Near monochromatic ducted gravity waves associated with a convective sytem close to the Pyrenées, Q. J. R. Meteorol. Soc., 141, 1320–1332, doi:10.1002/qj.2441, ~~2014.~~ 2015d.

Rotach, M. W., Calanca, P., Graziani, G., Gurtz, J., Steyn, D. G., Vogt, R., Andretta, M., Christen, A., Cieslik, S., Connolly, R., De Wekker, S. F. J., Galmarini, S., Kadygrov, E. N., Kadygrov, V., Miller, E., Neininger, B., Rucker, M., Van Gorsel, E., Weber, H., Weiss, A., and Zappa, M.: Turbulence structure and exchange processes in an Alpine Valley: The Riviera Project, Bull. Am. Meteorol. Soc., 85, 1367–1385, doi:10.1175/BAMS-85-9-1367, 2004.

Seaman, N. L., Gaudet, B. J., Stauffer, D. R., Mahrt, L., Richardson, S. J., Zielonka, J. R., and Wyngaard, J. C.: Numerical Prediction of Submesoscale Flow in the Nocturnal Stable Boundary Layer over Complex Terrain, Mon. Weather Rev., 140, 956–977, doi:10.1175/MWR-D-11-00061.1, 2012.

Skamarock, W., Klemp, J., Dudhi, J., Gill, D., Barker, D., Duda, M., Huang, X.-Y., Wang, W., and Powers, J.: A Description of the Advanced Research WRF Version 3, Tech. Rep., p. 113, doi:10.5065/D6DZ069T, 2008.

Smedman, A.-S., Bergström, H., and Högström, U.: Spectra, variances and length scales in a marine stable boundary layer dominated by a low level jet, Boundary-Layer Meteorol., 76, 211–232, doi:10.1007/BF00709352, 1995.

Soler, M., Infante, C., Buenestado, P., and Mahrt, L.: Observations of nocturnal drainage flows in a shallow gully, Boundary-Layer Meteorol., 105, 253–273, doi:10.1023/A:1019910622806, 2002.

Soler, M. R., Udina, M., and Ferreres, E.: Observational and Numerical Simulation Study of a Sequence of Eight Atmospheric Density Currents in Northern Spain, Boundary-Layer Meteorol., 153, 195–216, doi:10.1007/s10546-014-9942-2, http://link.springer.com/10.1007/s10546-014-9942-2, 2014.

Sorbjan, Z.: Structure of the Atmospheric Boundary Layer, Prentice Hall, Englewood Cliffs. 317 pp., New Jersey, 1989.

Steeneveld, G.-J.: Current challenges in understanding and forecasting stable boundary layers over land and ice, Frontiers in Environmental Science, 2, 41, 2014.

Stull, R. B.: An Introduction to Boundary Layer Meteorology, Kluwer Academic Publisher. 666 pp., 1988.

Sukoriansky, S., Dikovskaya, N., and Galperin, B.: Transport of momentum and scalar in turbulent flows with anisotropic dispersive waves, Geophys. Res. Lett., 36, 3–7, doi:10.1029/2009GL038632, 2009.

Sun, J., Burns, S. P., Lenschow, D. H., Banta, R., Newsom, R., Coulter, R., Frasier, S., Ince, T., Nappo, C., Cuxart, J., Blumen, W., Lee, X., and Hu, X. Z.: Intermittent turbulence associated with a density current passage in the stable boundary layer, Boundary-Layer Meteorol., 105, 199–219, doi:10.1023/A:1019969131774, 2002.

Sun, J., Lenschow, D. H., Burns, S. P., Miller, D., and Skelly, B.: Turbulence in Nocturnal Boundary Layers, Boundary-Layer Meteorol., 110, 255–279, 2004.

Sun, J., Mahrt, L., Banta, R. M., and Pichugina, Y. L.: Turbulence Regimes and Turbulence Intermittency in the Stable Boundary Layer during CASES-99, J. Atmos. Sci., 69, 338–351, doi:10.1175/JAS-D-11-082.1, 2012.

Sun, J., Mahrt, L., Nappo, C.~~–~~, and Lenschow, D. H.: Wind and temperature oscillations generated by wave–turbulence interactions in the stably stratified boundary layer, Journal of the Atmospheric Sciences, 72, 1484–1503, 2015a.

Sun, J., Nappo, C. J., Mahrt, L., Belusic, D., Grisogono, B., Stauffer, D. R., Pulido, M., Staquet, C., Jiang, Q., Pouquet, A., Yagüe, C., Galperin, B., Smith, R. B., Finnigan, J. J., Mayor, S. D., Svensson, G., Grachev, A. A., and Neff, W. D.: Review of Wave-Turbulence Interactions in the Stable Atmospheric Boundary Layer, Submitted to Rev. Geophys., ~~2015.~~ 2015b.

Terradellas, E., Morales, G., Cuxart, J., and Yagüe, C.: Wavelet methods: application to the study of the stable atmospheric boundary layer under non-stationary conditions, Dynamics of atmospheres and oceans, 34, 225–244, 2001.

Torrence, C. and Compo, G. P.: A Practical Guide to Wavelet Analysis, Bull. Am. Meteorol. Soc., 79, 61–78, doi:10.1175/1520-0477(1998)079<0061:APGTWA>2.0.CO;2, 1998.

Udina, M., Soler, M. R., Viana, S., and Yagüe, C.: Model simulation of gravity waves triggered by a density current, Q. J. R. Meteorol. Soc., 139, 701–714, doi:10.1002/qj.2004, http://DOI.wiley.com/10.1002/qj.2004, 2013.

van de Boer, A., Moene, A. F., Graf, A., Schüttemeyer, D., and Simmer, C.: Detection of Entrainment Influences on Surface-Layer Measurements and Extension of Monin-Obukhov Similarity Theory, Boundary-Layer Meteorol., 152, 19–44, doi:10.1007/s10546-014-9920-8, 2014.

Van de Wiel, B. J. H., Moene, A. F., Hartogensis, O. K., De Bruin, H. A. R., and Holtslag, A. A. M.: Intermittent Turbulence in the Stable Boundary Layer over Land. Part III: A Classification for Observations during CASES-99, J. Atmos. Sci., 60, 2509–2522, doi:10.1175/1520-0469(2003)060<2509:ITITSB>2.0.CO;2, 2003.

van den Kroonenberg, A. and Bange, J.: Turbulent flux calculation in the polar stable boundary layer: Multiresolution flux decomposition and wavelet analysis, J. Geophys. Res. Atmos., 112, 1–12, doi:10.1029/2006JD007819, 2007.

Van der Velde, I., Steeneveld, G., Wichers Schreur, B., and Holtslag, A.: Modeling and forecasting the onset and duration of severe radiation fog under frost conditions, Mon. Weather Rev., 138, 4237–4253, 2010.

Vercauteren, N. and Klein, R.: A clustering method to characterize intermittent bursts of turbulence and submeso motions interaction in the stable boundary layer., J. Atmos. Sci., doi:http://dx.doi.org/10.1175/JAS-D-14-0115.1, 2014.

Viana, S., Yagüe, C., and Maqueda, G.: Propagation and effects of a mesoscale gravity wave over a weakly-stratified nocturnal boundary layer during the SABLES2006 field campaign, Boundary-Layer Meteorol., 133, 165–188, doi:10.1007/s10546-009-9420-4, http://www.springerlink.com/index/10.1007/s10546-009-9420-4, 2009.

Viana, S., Terradellas, E., and Yagüe, C.: Analysis of Gravity Waves Generated at the Top of a Drainage Flow, J. Atmos. Sci., 67, 3949–3966, doi:10.1175/2010JAS3508.1, 2010.

Viana, S., Yagüe, C., and Maqueda, G.: Vertical structure of the stable boundary layer detected by RASS-SODAR and in-situ measurements in SABLES 2006 field campaign, Acta Geophys., 60, 1261–1286, doi:10.2478/s11600-011-0072-7, http://www.springerlink.com/index/10.2478/s11600-010-0072-7, 2012.

Vickers, D. and Mahrt, L.: The cospectral gap and turbulent flux calculations, J. Atmos. Ocean. Technol., 20, 660–672, doi:10.1175/1520-0426(2003)20<660:TCGATF>2.0.CO;2, 2003.

Vindel, J. M. and Yagüe, C.: Intermittency of Turbulence in the Atmospheric Boundary Layer: Scaling Exponents and Stratification Influence, Boundary-Layer Meteorol., 140, 73–85, doi:10.1007/s10546-011-9597-1, 2011.

Voronovich, V. and Kiely, G.: On the gap in the spectra of surface-layer atmospheric turbulence, Boundary-Layer Meteorol., 122, 67–83, doi:10.1007/s10546-006-9108-y, 2007.

Whiteman, C.: Mountain Meteorology: Fundamentals and Applications, Oxford University Press. 355 pp., New Jork, 2000.

Whiteman, C. D., Hoch, S. W., Hahnenberger, M., Muschinski, A., Hohreiter, V., Behn, M., Cheon, Y., Zhong, S., Yao, W., Fritts, D., et al.: METCRAX 2006: Meteorological experiments in Arizona's Meteor crater, Bull. Am. Meteorol. Soc., 89, 1665–1680, 2008.

Yagüe, C., Viana, S., Maqueda, G., and Redondo, J. M.: Influence of stability on the flux-profile relationships for wind speed, Φ m, and temperature, Φ h, for the stable atmospheric boundary layer, Nonlin. Processes Geophys., 13, 185–203, 2006.

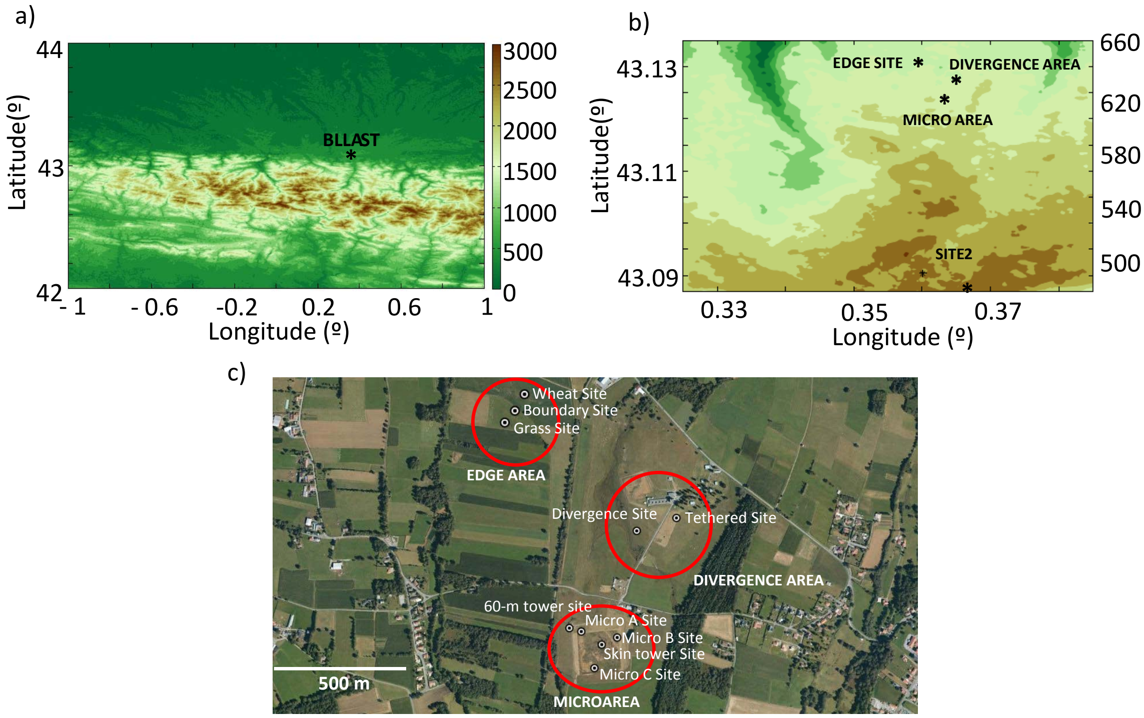

Figure 1. a) Topographic map of Pyrenees area around BLLAST~~campaign areas and sites used in this study~~. ~~Note that Super-Area 2 was located 4 km south from Micro~~ b) Topographic map of BLLAST area. c) Aerial view of BLLAST sites (except Area 2). NOTE - Figures a and ~~it is not shown in this map~~b from Routine ASTER Global Digital Elevation Model from NASA Land Processes Distributed Active Archive Center (LP DAAC). ~~From~~ Figure c from Google Earth.

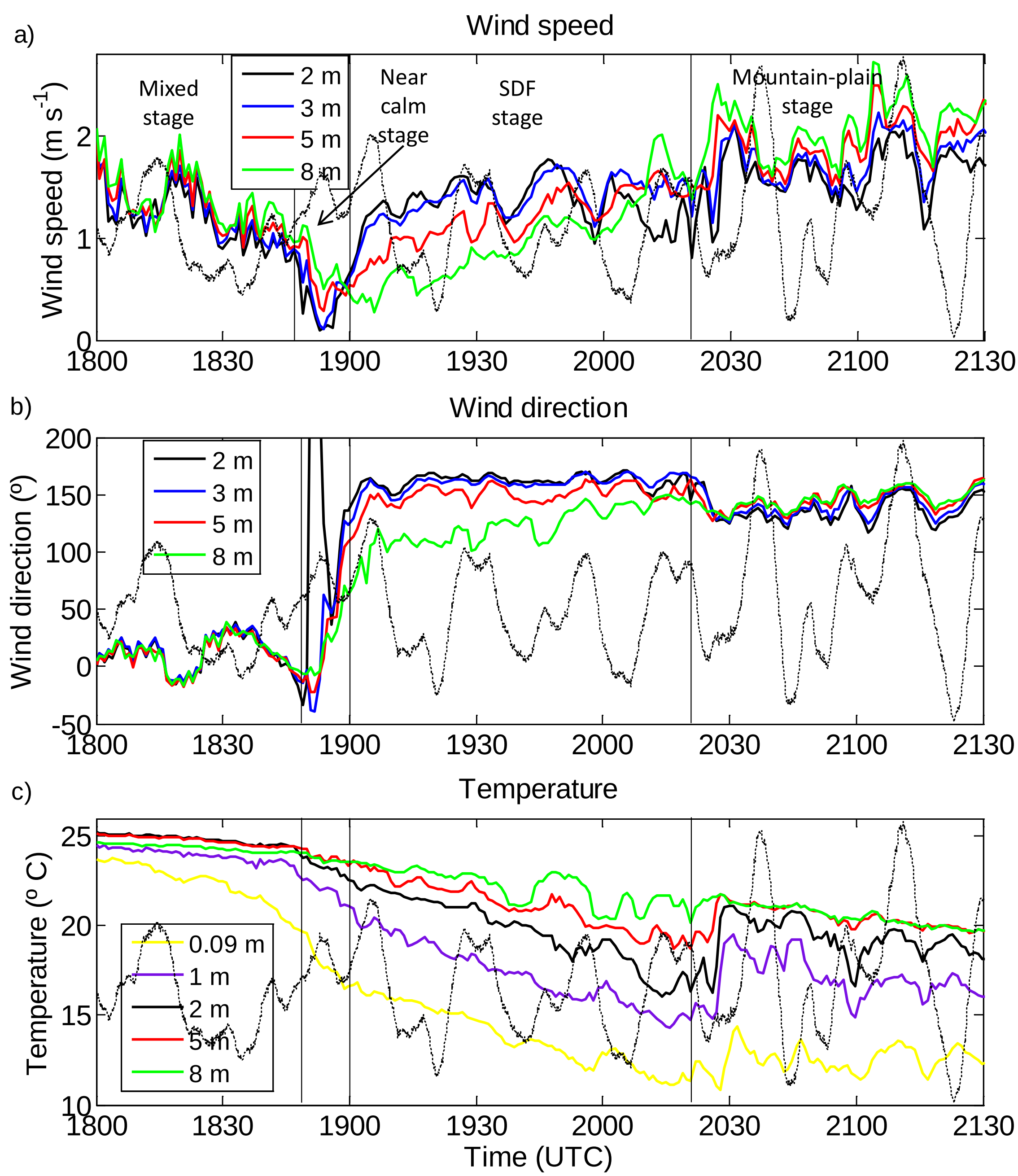

Figure 2. Time series from sonic anemometers and thermocouples measurements at the Divergence Site. a) Wind speed (m s^{-1}). (b) Wind direction (º). (c) Temperature (ºC). Note that filtered surface pressure from Micro A is overlaid for reference with thin dotted black line.

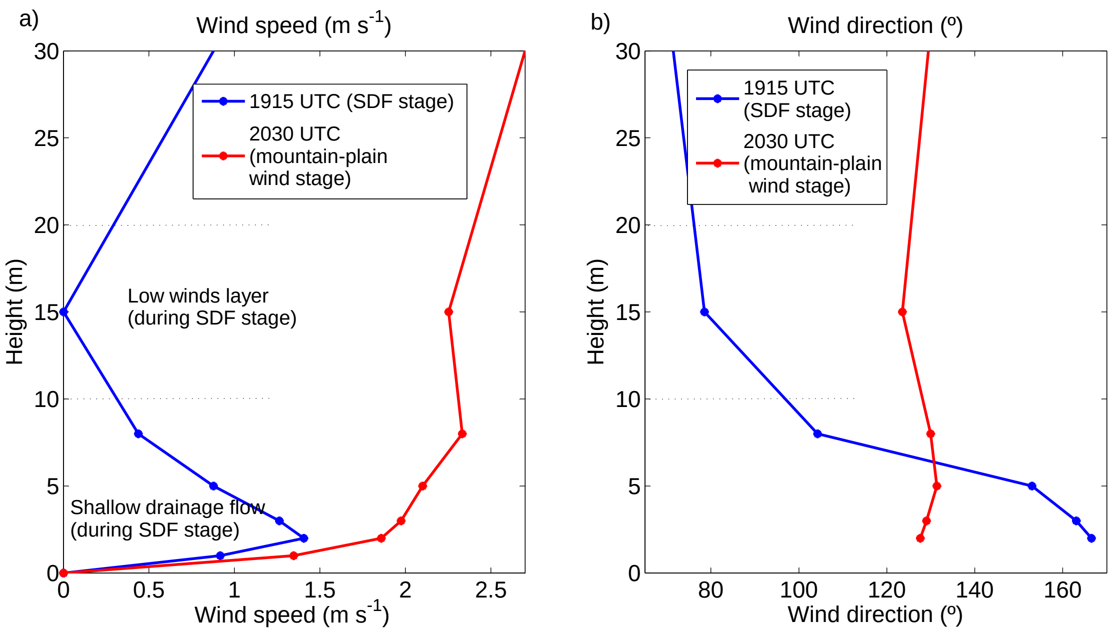

Figure 3. Wind speed (a) (m s^{-1}) and wind direction (b) (º) vertical profiles during shallow drainage flow (SDF) stage at 1915 UTC (blue line) and during mountain-plain wind stage at 2030 UTC (red line). Measurements from Divergence site and 60-m tower site instruments.

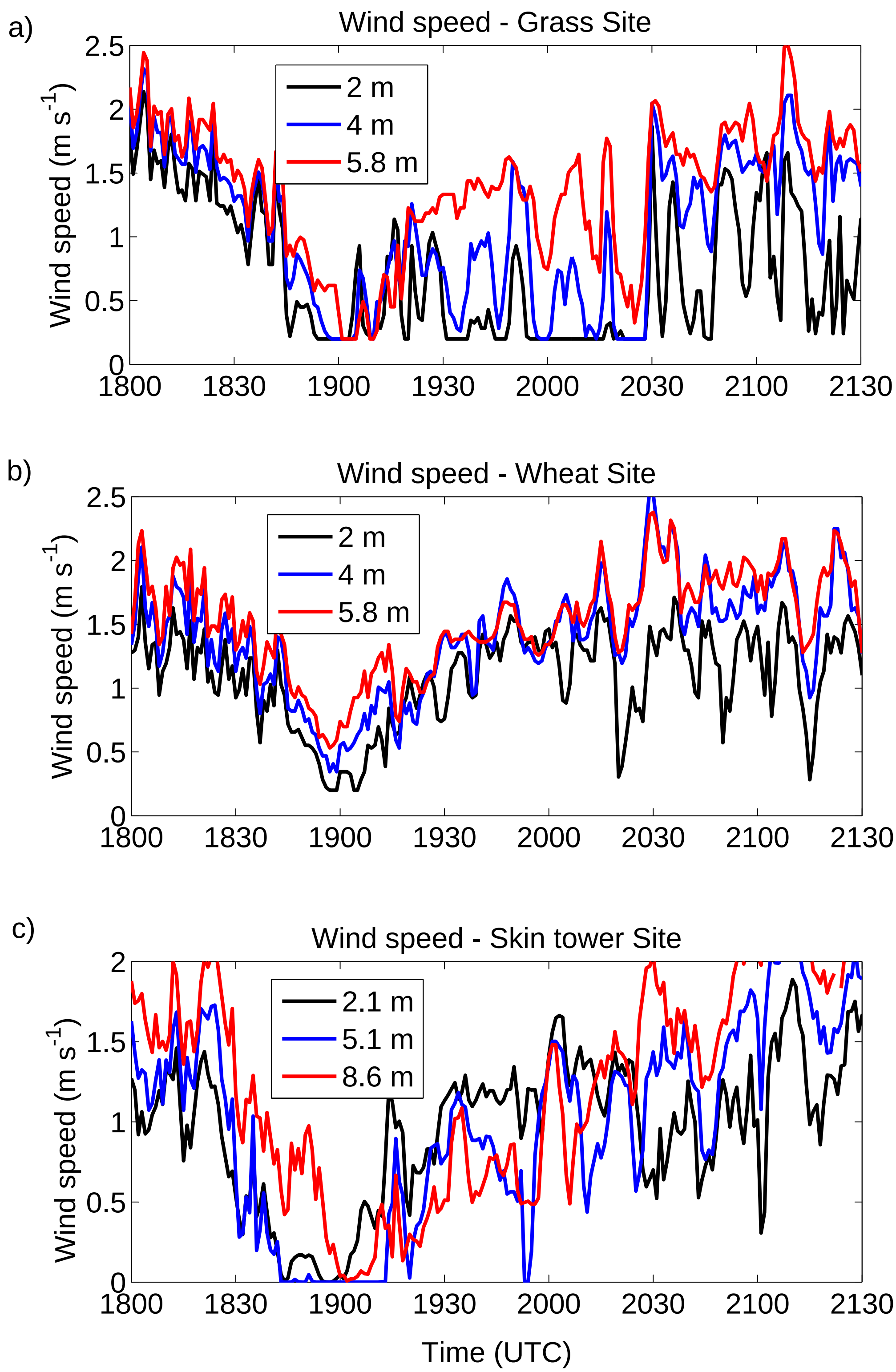

Figure 4. Wind speed (m s^{-1}) measured at different heights at the Grass Site (a), Wheat Site (b) and Skin tower Site (Micro Area) (c).

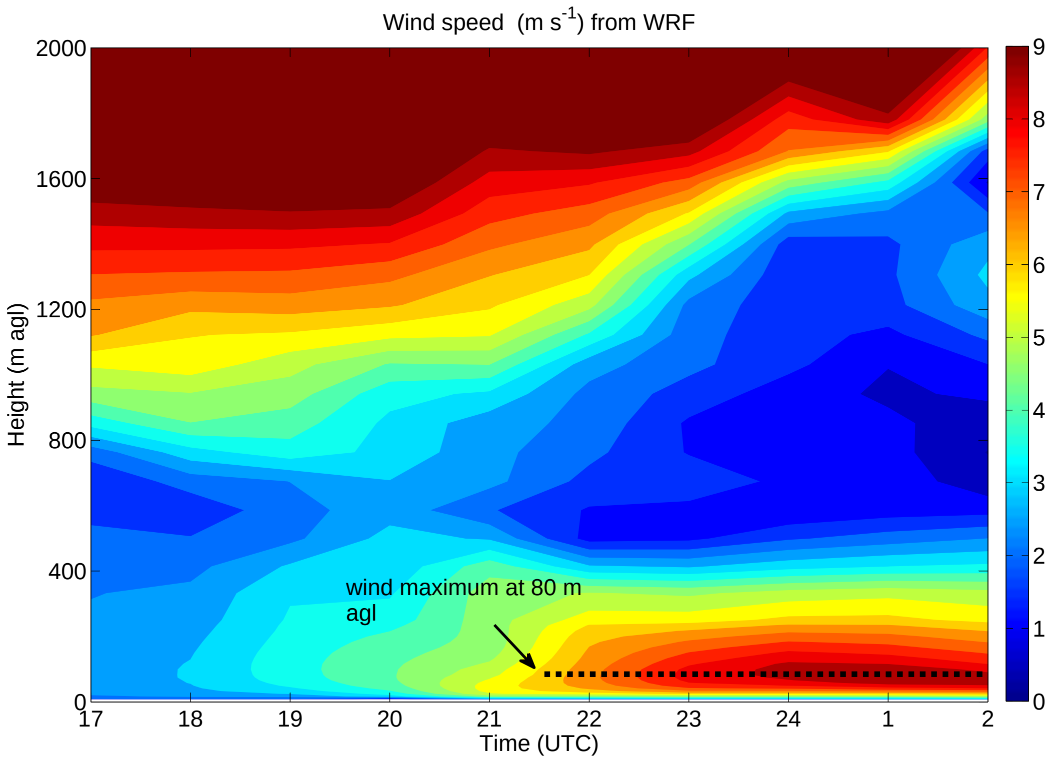

Figure 5. WRF wind speed (m s^{-1}) over Lannemezan from 1700 UTC of 2nd July to 0200 UTC of 3rd July from surface to 2000 m agl. The results indicate the appearance of the mountain-plain wind in the lowest meters.

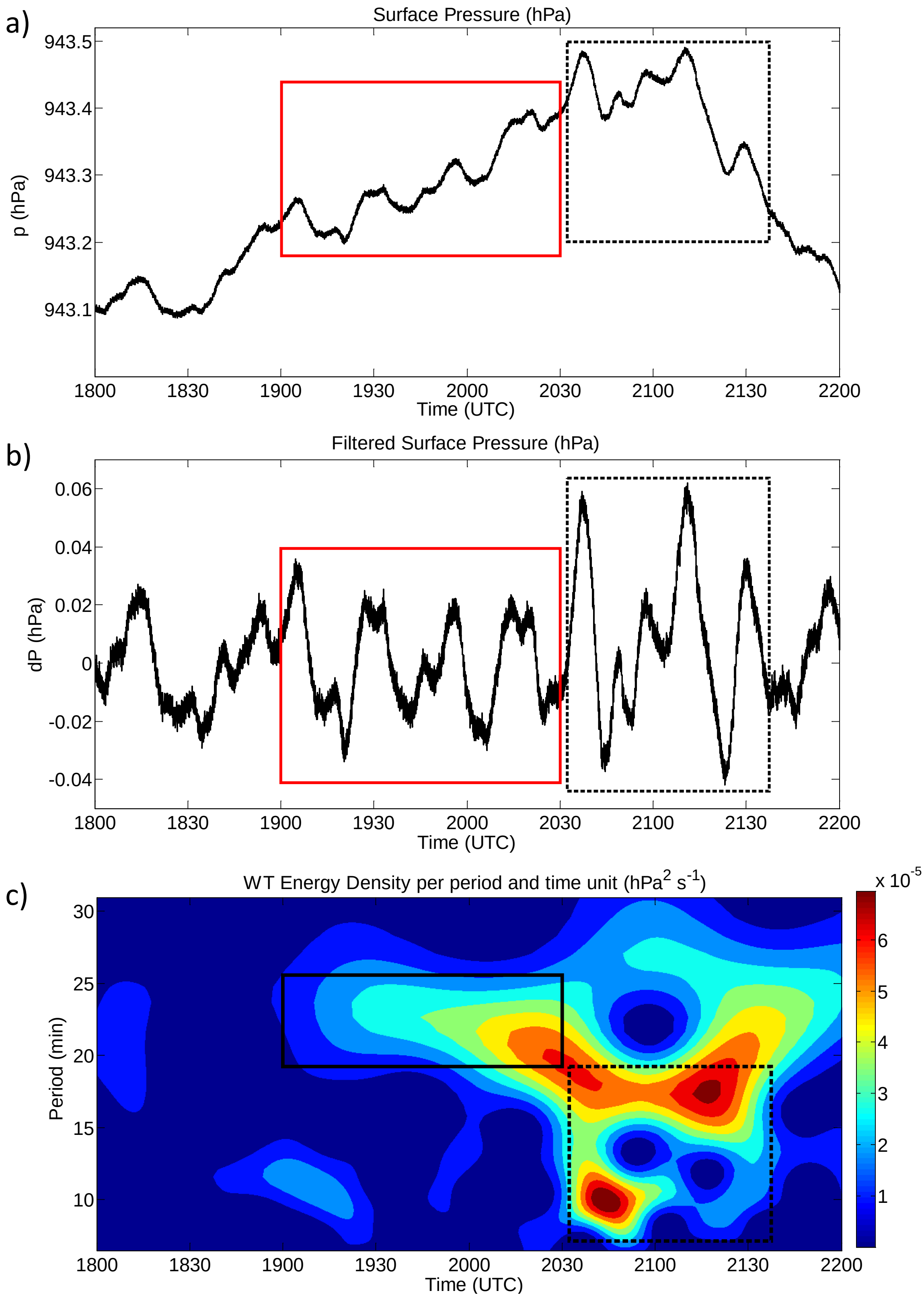

Figure 6. Absolute (a) and filtered (b) surface pressure (hPa) measured by microbarometer A. c) Morlet wavelet-based energy density (hPa^2 s^{-1}). Wave event 1 is indicated with red rectangles (black in c) and Wave event 2 with dashed ~~purple~~ black rectangles. Note: these figures are almost identical for microbarometers B and C.

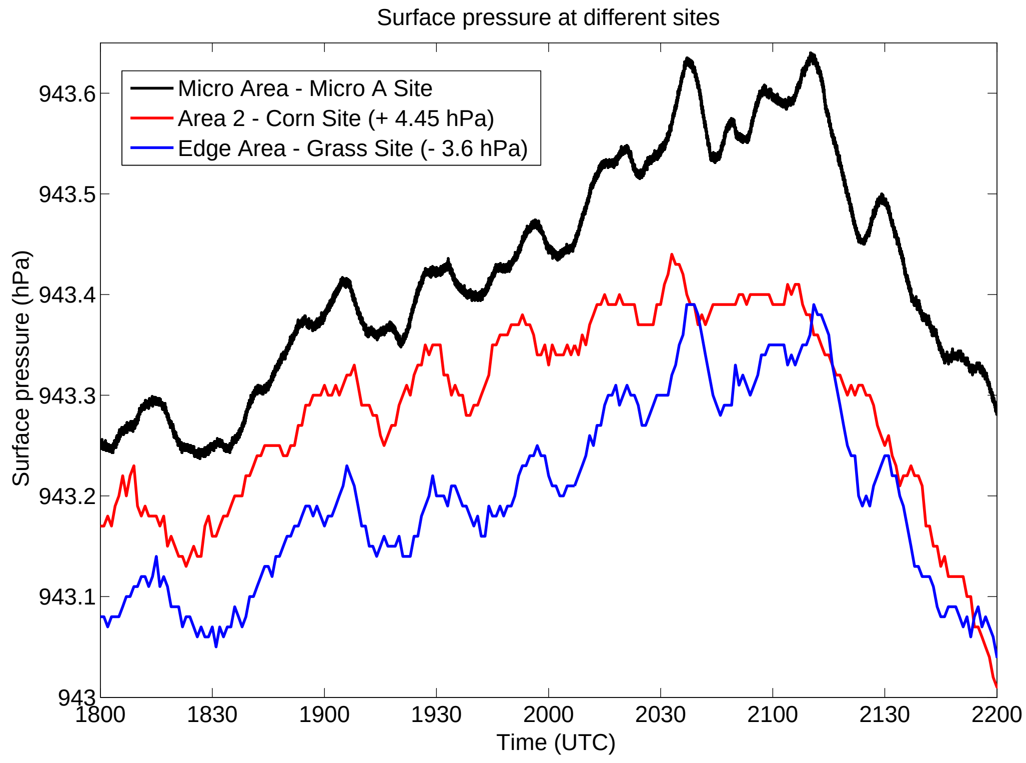

Figure 7. Absolute pressure (hPa) observed at three different sites of BLLAST: Micro A Site at Micro Area (black line), Corn Site at SS2 Area (red line, 3.8 km S from Micro A Site) and Grass Site at the Edge Area (blue line, 1 km NNW from Micro A Site). Note that 4.45 (3.6) hPa have been added (subtracted) to the original value at Corn site (Grass site) in order to compare the figures.

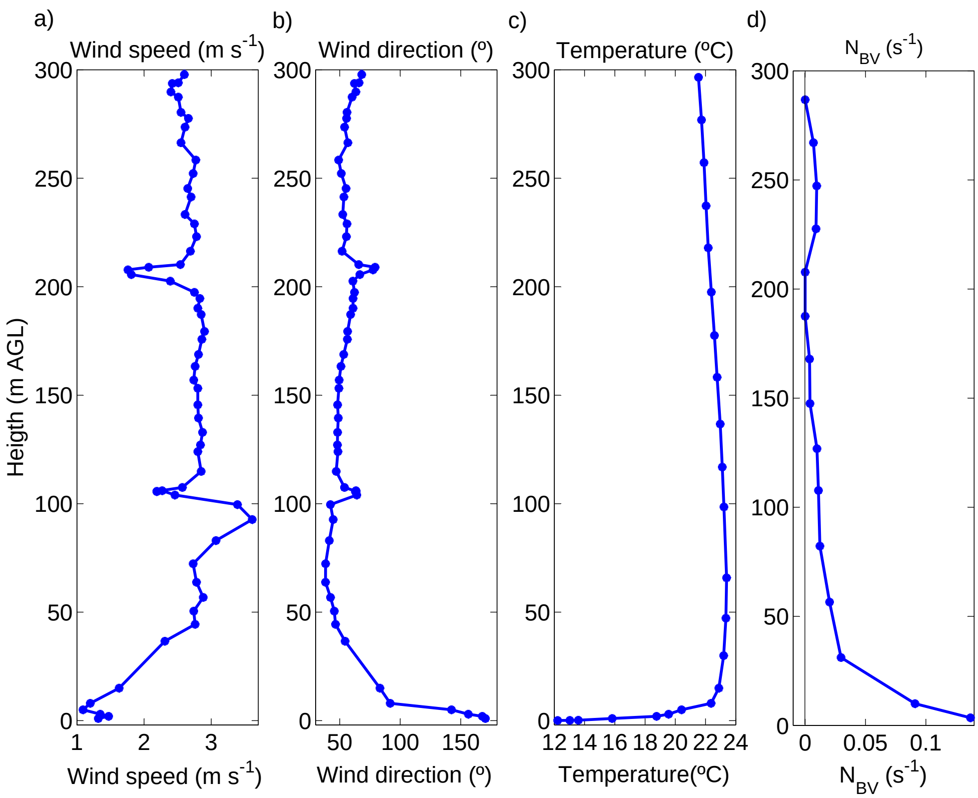

Figure 8. Vertical profiles considering combination of measurements from 8-m tower measurements (from 1 m to 8 m agl), 60-m tower measurements (15 m agl) and tethered balloon´s descent measurements (~~around 1955 UTC~~from 30 m up to 300 m agl) ~~and 8-m and 60-m tower measurements~~ approximately at ~~the same time~~1955 UTC. a) Wind speed (m s^{-1}). b) Wind direction (º). c) Temperature (º C). d) Brunt Väisälä frequency (N_{BV}) (s^{-1}).~~Horizontal black line in Figure d shows the height where N_{BV} becomes 0 and therefore, the SBL upper limit, where gravity waves are trapped.~~

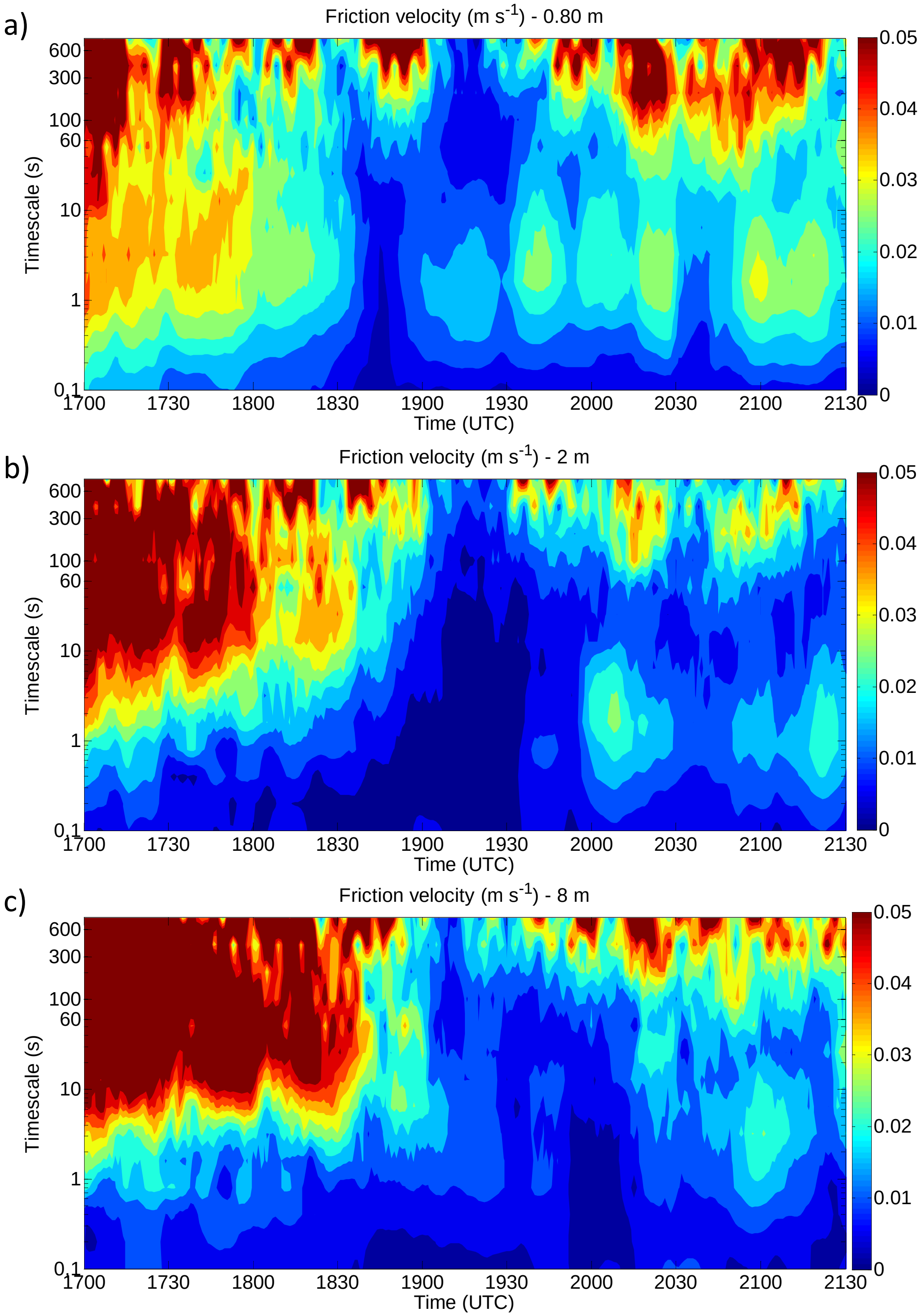

Figure 9. Multi-Resolution Flux Decomposition (MRFD) of the friction velocity (m s^{-1}) at 0.8 m agl (a), 2 m agl (b) and 8 m agl (c) at the Divergence Site.

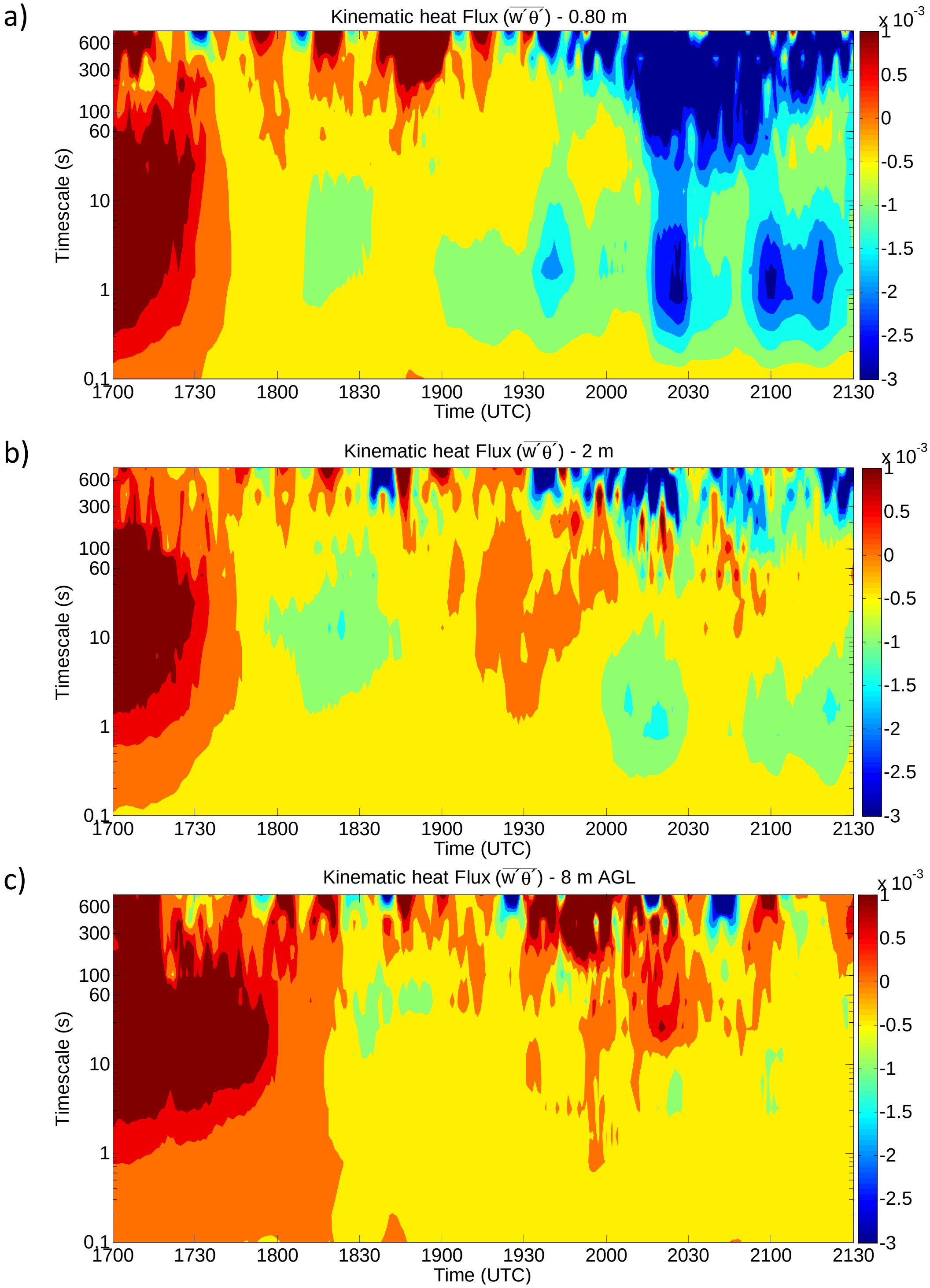

Figure 10. Multi-Resolution Flux Decomposition (MRFD) of kinematic heat flux (K m s^{-1}) at 0.8 m agl (a), 2 m agl (b) and 8 m agl (c) at the Divergence Site.

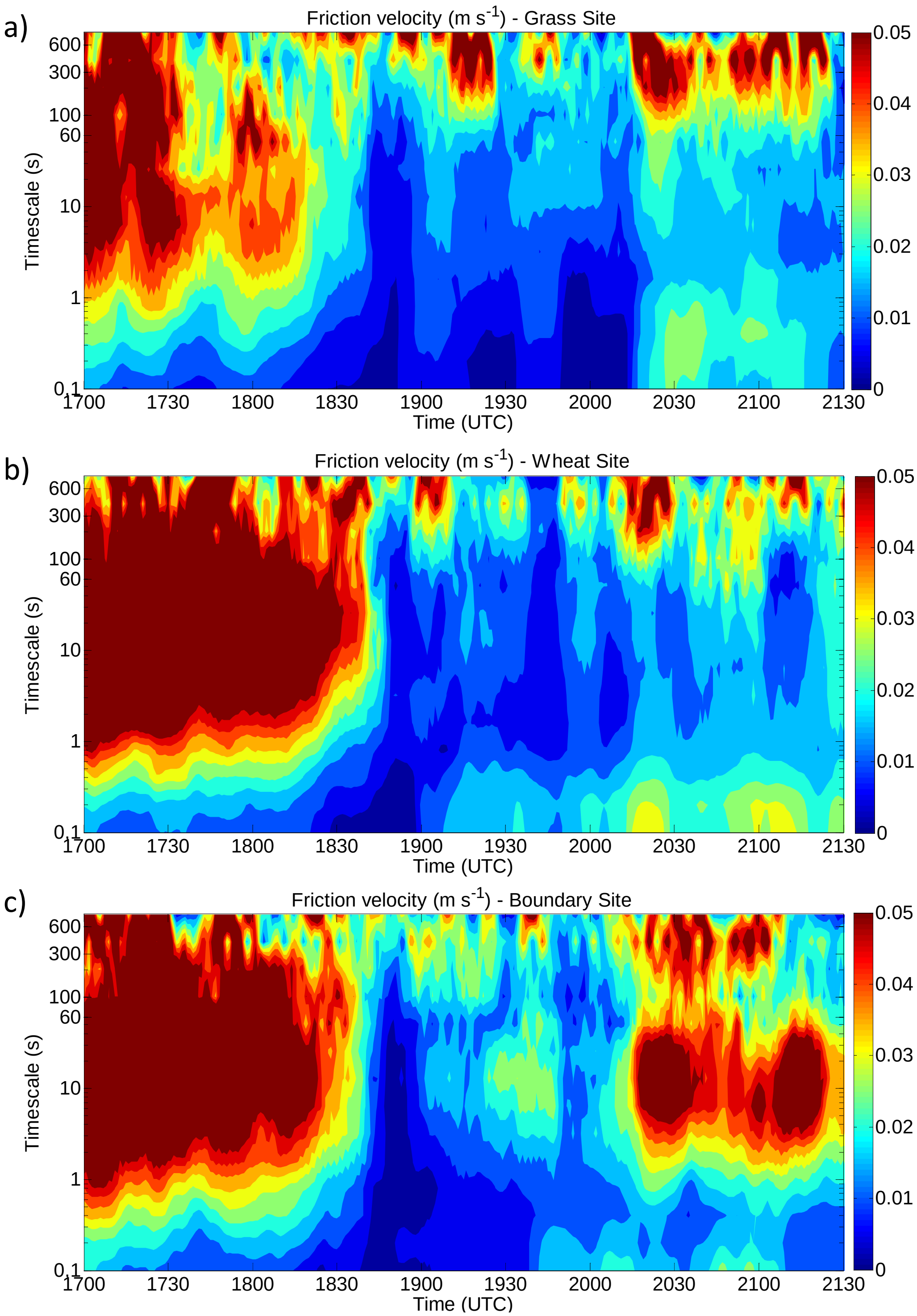

Figure 11. Multi-Resolution Flux Decomposition (MRFD) of the friction velocity (m s^{-1}) at Grass (a), Wheat (b) and Boundary (c) Sites (located at Edge Area and at 2 m agl).

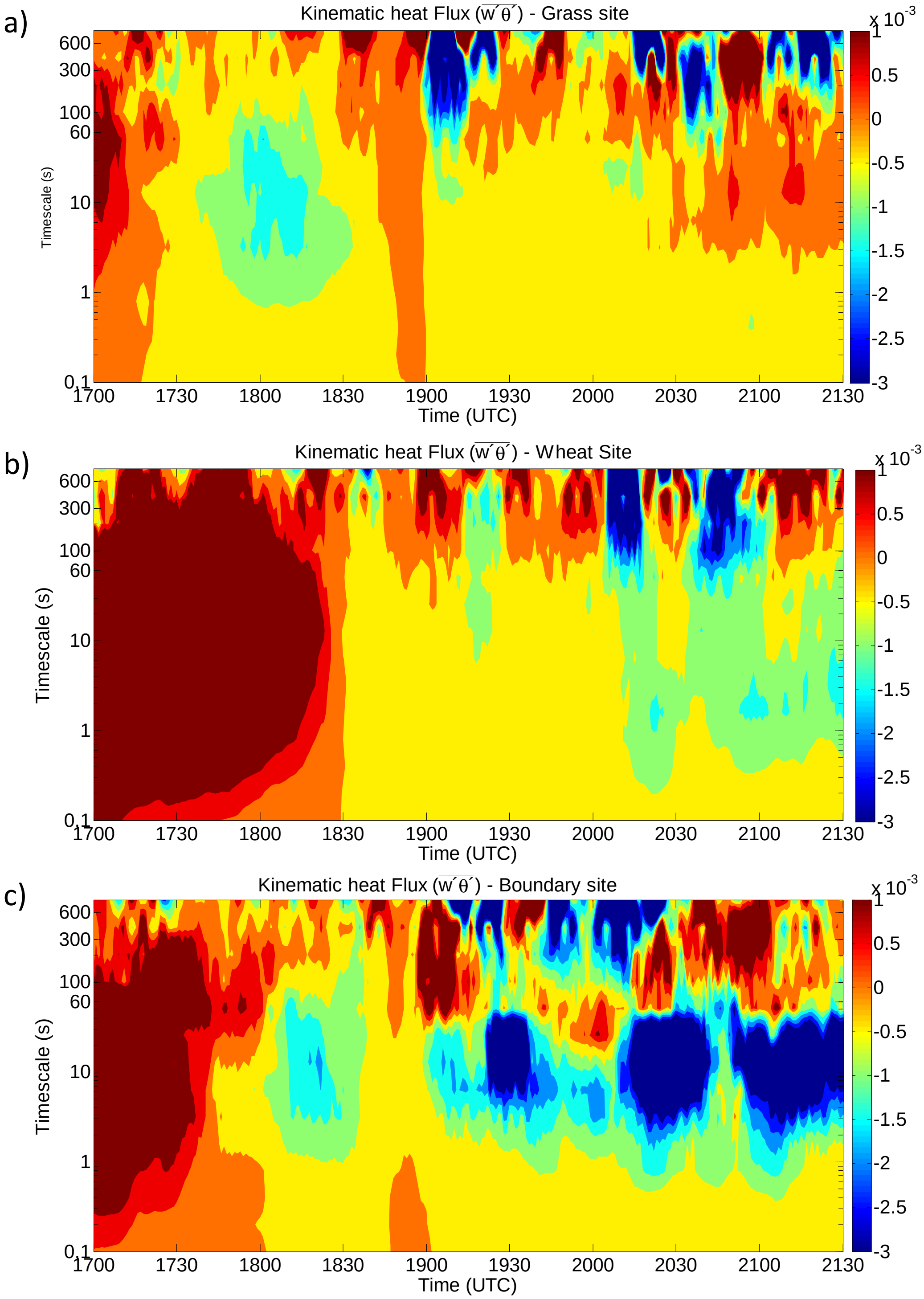

Figure 12. Multi-Resolution Flux Decomposition (MRFD) of kinematic heat flux (K m s^{-1}) at Grass (a), Wheat (b) and Boundary (c) Sites (located at Edge Area and at 2 m agl).

Table 1. Characteristics of BLLAST sites considered in this study.

Super-Area	Area	Site	Location	Height asl
SUPER-AREA 1	Micro Area	Micro A Site	43º 07' 26,8" N 00º 21' 46,9" E	602 m
		Micro B Site	43º 07' 25,9" N 00º 21' 53,1" E	600 m
		Micro C Site	43º 07' 22,2" N 00º 21' 49,2" E	601 m
		Skin-tower Site	43º 07' 25,1" N 00º 21' 50,4" E	600 m
		60-m tower Site	43º 07' 27,1" N 00º 21' 45,1" E	602 m
	Divergence Area	Divergence Site	43º 07' 39,1" N 00º 21' 56,3" E	590 m
		Tethered Site	43º 07' 40,6" N 00º 22' 03,1" E	594 m
	Edge Area	Grass Site	43º 07' 52,5" N 00º 21' 33,9" E	582 m
		Wheat Site	43º 07' 56,1" N 00º 21' 37,3" E	582 m
		Boundary Site	43º 07' 54,1" N 00º 21' 35,6" E	582 m
SUPER-AREA 2	Area 2	Corn Site	43º 05' 25,1" N 00º 21' 29,6" E	646 m
		Moor Site	43º 05' 24,9 " N 00º 21' 42,6" E	646 m

Table 2. Instrumentation used in each site.

Area	Site	Instruments
Micro Area	Micro A Site	Microbarometer PAROSCIENTIFIC
	Micro B Site	Microbarometer PAROSCIENTIFIC
	Micro C Site	Microbarometer PAROSCIENTIFIC
	Skin-tower Site	8-m tower Site (thermometers, wind vanes)
	60m-tower Site	60-m tower Site (thermometers, wind vanes)
Divergence Area	Divergence Site	8-m tower (thermocouples, sonic anemometers)
	Tethered Site	Tethered balloon (thermometers, wind vanes)
Edge Area	Grass Site	8-m tower (thermometers, sonic anemometers and P from LICOR)
	Wheat Site	8-m tower (thermometers, sonic anemometers)
	Boundary Site	Sonic anemometer
Area 2	Corn Site	Pressure data from LICOR barometer

Table 3. Gravity waves parameters evaluated from filtered surface pressure records of three microbarometers. Uncertainty is indicated inside brackets (range of values). Note how uncertainty is lower for wave event 2.

	Time (UTC)	Period (min)	Wavelength (km)	Phase speed (m s^{-1})	Direction of propagation (
Wave event 1	1925 - 2000	20 - 25	not ~~well defined~~ well-defined	not ~~well defined~~ well-defined	not ~~well defined~~ well-define
	2005 - 2025	22 - 24	[23 - 30]	[17 - 19]	[80 - 90]
Wave event 2	2035 - 2055	10,5 - 12	~~13~~ [12 - 15]	~~–~~[18 - 20]	~~80~~ [75 - 95]
	2105 - 2130	16 -21	~~9~~ [7 ~~,5~~ - 10]	~~40~~ [6 - 9]	[32 - 42]